Fixed point theory of iterative excitation schemes in NMR

R. Tycko[a] and A. Pines
Department of Chemistry, University of California, and Materials and Molecular Research Division, Lawrence Berkeley Laboratory, Berkeley, California 94720

J. Guckenheimer[b]
Department of Mathematics, University of California, Santa Cruz, California 95064

(Received 17 May 1985; accepted 11 June 1985)

Iterative schemes for NMR have been developed by several groups. A theoretical framework based on mathematical dynamics is described for such iterative schemes in nonlinear NMR excitation. This is applicable to any system subjected to coherent radiation or other experimentally controllable external forces. The effect of the excitation, usually a pulse sequence, can be summarized by a propagator or superpropagator (U). The iterative scheme (F) is regarded as a map of propagator space into itself, $U_{n+1} = FU_n$. One designs maps for which a particular propagator $\bar{U}$ or set of propagators $\{\bar{U}\}$ is a fixed point or invariant set. The stability of the fixed points along various directions is characterized by linearizing F around the fixed point, in analogy to the evaluation of an average Hamiltonian. Stable directions of fixed points typically give rise to broadband behavior (in parameters such as frequency, rf amplitude, or coupling constants) and unstable directions to narrowband behavior. The dynamics of the maps are illustrated by "basin images" which depict the convergence of points in propagator space to the stable fixed points. The basin images facilitate the optimal selection of initial pulse sequences to ensure convergence to a desired excitation. Extensions to iterative schemes with several fixed points are discussed. Maps are shown for the propagator space $SO(3)$ appropriate to iterative schemes for isolated spins or two-level systems. Some maps exhibit smooth, continuous dynamics whereas others have basin images with complex and fractal structures. The theory is applied to iterative schemes for broadband and narrowband π (population inversion) and $\pi/2$ rotations, MLEV and Waugh spin decoupling sequences, selective n-quantum pumping, and bistable excitation.

I. INTRODUCTION

The development of new techniques in nuclear magnetic resonance (NMR) is often synonymous with the development of new radio frequency (rf) pulse sequences or excitation schemes. A similar statement is recently becoming applicable to other areas of spectroscopy, for example, coherent laser spectroscopy and electron paramagnetic resonance. This paper is concerned with a fairly recent approach to developing pulse sequences, namely the use of iterative schemes.[1-6]

In general terms, the purpose of a pulse sequence in NMR is to bring about some desired response or evolution of a nuclear spin system. The effect of a pulse sequence is described quantum mechanically by a propagator or evolution operator.[7(a)] Pulse sequences of several types are treated in this paper. One type of sequence can be termed a broadband excitation sequence.[1,5-20] Such a sequence causes a spin system to evolve from an initial condition of thermal equilibrium to a final, nonequilibrium condition, e.g., a condition of population inversion, uniformly over a large range of values of some experimental parameter. Possible experimental parameters include the rf frequency,[1,7,9-11,13-15,17,18] the rf field amplitude,[1,5-9,11,13-16,18] and spin coupling strengths.[8,12,19] A second type of sequence can be called a narrowband excitation sequence.[1,6] Such a sequence causes a spin system to evolve to a desired final condition only over a small range of values of some experimental parameter. Narrowband excitation is useful in many contexts including spatial localization of NMR signals.[6,20-22] A third type of sequence is used for spin decoupling. A decoupling sequence causes a coupled spin system to evolve as if certain couplings were absent. Homonuclear decoupling sequences[23-31] effectively remove couplings between like spins, i.e., the same isotope; heteronuclear decoupling sequences[3,4,32-38] remove couplings between unlike spins, i.e., different isotopes. A fourth type of sequence is used for the excitation of multiple quantum coherences in coupled spin systems[39-42]; in other words, coherences between spin states for which the difference Δm between their Zeeman quantum numbers is not equal to ± 1. Of particular interest is the excitation only of coherences for which Δm is a multiple of a given integer n, called nk-quantum selective excitation.[2,40]

In addition to the four general types of pulse sequences mentioned above, there are numerous other types of sequences which produce other useful and interesting responses, such as polarization transfer[43-46] and time reversal.[47] The majority of rf pulse sequences developed to date, despite their different functions, have a common feature: they are developed by some form of pulse-by-pulse analysis of specific sequences. A variety of theoretical tools have been applied to such pulse-by-pulse analyses, including the Bloch vector[48] formalism and the related fictitious spin-1/2[49-51] and product operator[52,53] formalisms. A particularly powerful approach to the analysis of specific sequences is provided

[a] Current address: Department of Chemistry, University of Pennsylvania, Philadelphia, PA 19104.
[b] Current address: Department of Mathematics, Cornell University, Ithaca, NY 14853.

 0021-9606/85/182775-28$02.10

by average Hamiltonian theory.[23,24,26] With average Hamiltonian theory, the propagators for specific sequences or for a parametrized set of sequences[7–9] may be calculated. A search for a sequence with the desired propagator may be carried out with the help of experience, intuition, and inspiration, or based on numerical methods. In general, this is a difficult problem due to the inherently nonlinear nature of the problem, namely the impossibility of directly inverting the response to obtain the necessary excitation.

The detailed analysis of specific sequences is a useful approach, provided that the sequences are composed of a small number of individual pulses. However, there are cases in which such an approach is not sufficient. These are cases, such as the four types of pulse sequences briefly described above, in which the desired response cannot be achieved satisfactorily with pulse sequences that are simple enough to be analyzed in detail, but can be achieved with more complex sequences. A conceptually different approach to pulse sequence design is then required. One such approach is the use of iterative schemes, as depicted schematically in Fig. 1. Rather than attempting to derive a sequence with the desired propagator directly, a set of operations is defined that may be applied repetitively to an initial pulse sequence S_0, generating a series of iterate sequences S_1, S_2, S_3, etc. The theoretical task is to construct the operations in such a way that the propagators for the iterate sequences converge to the desired form. Operations treated in the literature include phase shifting of rf pulses,[1–6] permutation of pulses,[3–4] formation of inverse sequences,[5,6] and concatenation of sequences.[1–6] Typically, the higher iterate sequences are successively longer and are composed of increasing numbers of individual pulses. If an iterative scheme is successful, the higher iterates produce the desired response with increasing fidelity. In addition, the qualitative features of the response produced by the iterate sequences are largely independent of the choice of the initial sequence. For example, under a given scheme S_5 may always be a broadband excitation sequence, regardless of S_0. *Thus, the development and evaluation of an iterative scheme must focus on the operations that comprise the scheme, rather than on the specific sequences that the scheme generates.*

In this paper, we present a geometrical framework for analyzing and developing iterative schemes. The underlying philosophy of the approach is to treat an iterative scheme as a function F that acts on the space of all possible pulse sequence propagators, mapping the propagator U_n for the sequence S_n onto the propagator U_{n+1} for the sequence S_{n+1}. Repeated applications of the iterative scheme then correspond to iterations of F. The study of the properties of iterated mappings is the domain of mathematical dynamics,[54,55] an extensive and active field whose physical applications extend to such areas as turbulence, nonlinear oscillations, and intramolecular energy transfer.[56] The framework for treating iterative schemes described below is based on principles of mathematical dynamics, leading to simple pictures that summarize the behavior of iterative schemes as well as algebraic and numerical methods for examining the behavior in detail. As shown below, the occurrence of fixed points of F is an essential and unifying feature of the dynamics of iterative schemes. For that reason, we refer to our approach as a fixed point theory of iterative excitation schemes.

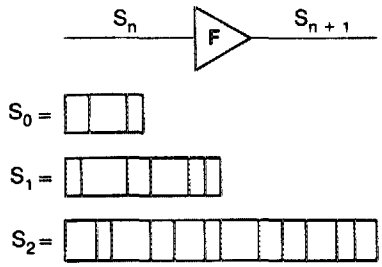

FIG. 1. Schematic illustration of an iterative scheme. Operations are applied repetitively to an initial pulse sequence S_0, generating a series of iterate sequences, S_1, S_2, etc. The iterate sequences typically become increasingly complex. The theoretical problem is to design the operations in such a way that the iterate sequences produce the desired excitation of a spectroscopic system to increasing degrees of accuracy.

The paper is organized as follows. Section II describes the interpretation of iterative schemes as mappings or functions on the space of propagators. The significance of fixed points is explained and demonstrated using a simple mathematical example as background for the later NMR examples. In Sec. III, the fixed point theory is applied to a class of iterative schemes that we and others have previously introduced for generating broadband and narrowband population inversion sequences for systems of isolated spins. Algebraic methods for analyzing the fixed point properties of the schemes are presented. In Sec. IV, specific schemes for broadband population inversion are treated. Numerical methods are developed that lead to a procedure for optimizing the performance of an iterative scheme by the proper choice of an initial sequence. In Sec. V, the fixed point theory is applied to schemes for generating narrowband population inversion sequences. In Sec. VI, brief treatments of iterative schemes developed by other authors are given with the purpose of demonstrating the applicability of the fixed point theory. In Sec. VII, a summary of the results of the fixed point theory and a discussion of potential further applications is given.

II. MATHEMATICAL BASIS OF THE FIXED POINT THEORY

A. Iterative schemes as functions on the propagator space

Consider a spin system with N independent quantum mechanical states $|n\rangle$. Any operator that operates on the state of the system can be written as a unique linear combination of elements of a basis of N^2 independent operators, for example $|n\rangle\langle m|$, allowing complex coefficients. The space spanned by these N^2 basis operators is called Liouville space.[24,57] Hermitian operators, such as the Hamiltonian, the density operator, and observable operators, occupy a subset of Liouville space. Unitary operators occupy a different subset. The propagators that correspond to all possible pulse sequences or experimentally realizable operations on

the spin system, a special case of unitary operators, occupy a subset of Liouville space that we call the propagator space. The dimension and topology of the propagator space is determined not only by N, but also by the internal spin Hamiltonian. As an example, the propagator space for a quadrupolar spin-1 nucleus is an eight-dimensional space in general. However, if the quadrupole interaction identically vanishes, the propagator space reduces to three dimensions.

Consider a pulse sequence S_0, defined by a particular combination of rf phase and amplitude functions of time. For a given internal spin Hamiltonian, the propagator corresponding to S_0 is U_0. U_0 may be represented by a point in the propagator space. If an iterative scheme is applied to S_0, it generates a new pulse sequence S_1. The corresponding propagator, for the same internal spin Hamiltonian, is U_1, represented in general by a different point in the propagator space. As shown in Fig. 2, further iterations produce a series of points in the propagator space. Let us assume that there is a function F associated with the iterative scheme which generates that series of points according to the rule

$$U_{n+1} = FU_n. \tag{1}$$

In any experimental situation, a range of experimental parameters exists, arising, for example, from inhomogeneity of the applied rf and static magnetic fields and from variations in the internal spin interactions due to orientational or chemical heterogeneity. Then, since there is in general a distinct propagator for each distinct set of values of the experimental parameters, there exists in practice a locus of points in the propagator space for each sequence rather than a single point. F then maps the locus of points $\{U_n\}$ onto the locus of points $\{U_{n+1}\}$.

There is indeed a single, well-defined function associated with an iterative scheme under certain conditions. First, the scheme should be rigidly constructed so that, given the sequence S_n, there is only one possible sequence S_{n+1}. If the scheme is more flexible, allowing several possibilities for S_{n+1}, as is the case with some schemes in the literature,[3-5] then there may be several associated functions. Second, the series of propagators U_0, U_1, U_2, etc. should be determined only by U_0, the overall initial propagator, without reference to the details of the initial pulse sequence or of the internal Hamiltonian. Important cases where the second criterion is generally not satisfied are the iterative schemes for generating heternuclear decoupling sequences which depend on the permutation of pulses.[3,4] As will be shown in Sec. VI, a fixed point analysis still provides useful information in those cases, even though a function on the propagator space is not uniquely defined.

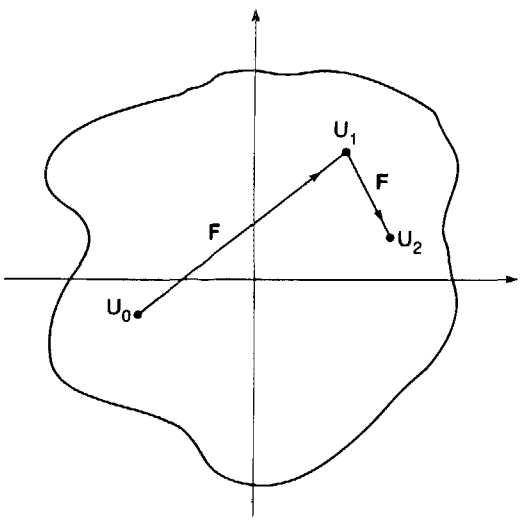

FIG. 2. The interpretation of an iterative scheme as a function or mapping on the propagator space. The propagators U_0, U_1, U_2, etc. for the pulse sequences S_0, S_1, S_2, etc. are described by points in an operator space. The underlying function F maps each point U_n onto its iterate U_{n+1}.

B. Significance of fixed points

The purpose of an iterative scheme is to generate pulse sequences that produce a desired spin response, i.e., implement a specific desired propagator or set of propagators. Therefore, an essential property of a successful iterative scheme is that, if the initial sequence S_0 produces the desired response, then all of the iterate sequences S_n also produce the desired response. In the simplest case in which there is only one propagator $\bar{U}$ describing the desired response, this means that $U_n = \bar{U}$ if $U_0 = \bar{U}$ as shown in Fig. 3(a). In other words,

$$\bar{U} = F\bar{U} \tag{2a}$$

or

$$\bar{U} = F^n\bar{U}, \tag{2b}$$

where F^n indicates n iterations of the function F. $\bar{U}$ is then said to be a fixed point of F. More generally, there may be a set of propagators $\{\bar{U}^{(i)}\}$ which produce the desired response, as shown in Figure 3(b). Then F will have the property that

$$\{\bar{U}^{(j)}\} = F\{\bar{U}^{(j)}\}. \tag{3}$$

In other words, F may map one propagator in the set to

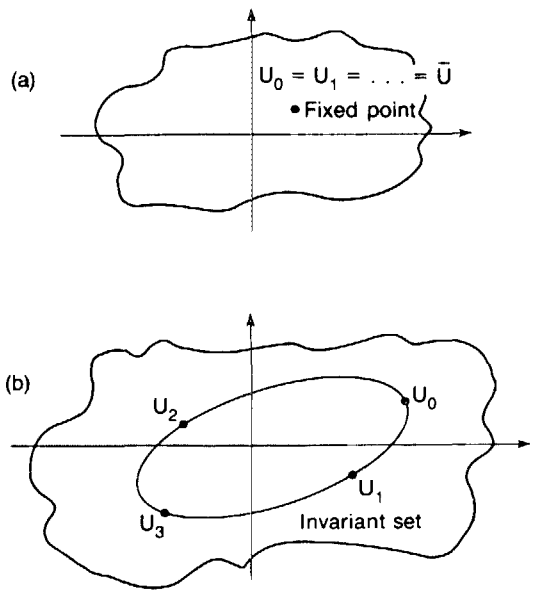

FIG. 3. The function F on the propagator space may have fixed points (a). These are points that are mapped onto themselves by F. More generally, F may have invariant sets (b). An invariant set is a set of points that is mapped onto itself. Under a successful iterative scheme, the fixed points or invariant sets represent propagators that accomplish the desired excitation.

another propagator in the set. $\{\bar{U}^{(i)}\}$ is said to be an invariant set of F. F may have several fixed points or invariant sets simultaneously.

A fixed point may be classified in terms of its stability as shown for the simplest case in Fig. 4. Roughly speaking, if points initially near the fixed point converge to the fixed point with successive iterations of F, the fixed point is said to be stable. Figure 4(a) illustrates a stable fixed point. An iterative scheme with a stable fixed point typically generates pulse sequences with broadband excitation properties. This is because a range of initial pulse sequence propagators, arising from a range of experimental parameters, converge to the desired propagator upon iteration. If points initially near the fixed point diverge from the fixed point with successive iterations of F, the fixed point is said to be unstable. Figure 4(b) illustrates an unstable fixed point. An iterative scheme with an unstable fixed point may generate pulse sequences with narrowband excitation properties. This is because only an initial pulse sequence propagator that exactly equals the desired propagator, arising from particular values of the experimental parameters, remains equal to the desired propagator upon iteration. Initial propagators that nearly equal the desired propagator progressively diverge from the desired propagator upon iteration. They may then converge to other, stable fixed points or remain nonconvergent.

It is also possible for a fixed point in a multidimensional space to be stable with respect to displacements in certain directions and unstable in other directions. Initial points near the fixed point may then approach the fixed point along a stable direction on low iterations before diverging along an unstable direction on higher iterations.

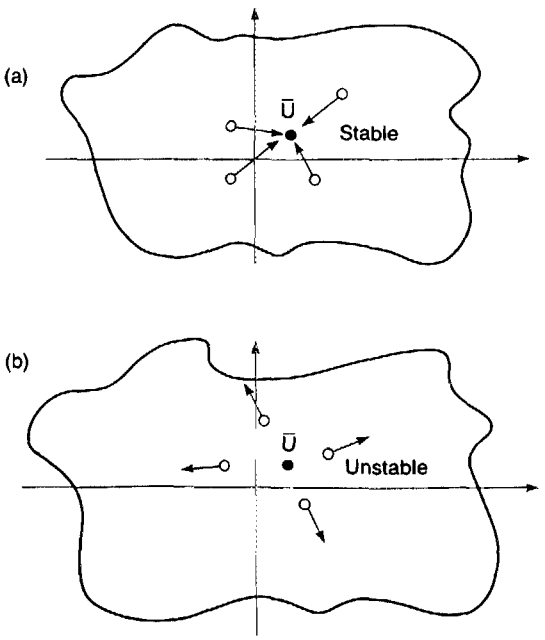

FIG. 4. Fixed points $\bar{U}$ of F may be stable or unstable. (a) Points near a stable fixed point converge to the fixed point with successive iterations of F. In this way, a desired propagator may be generated from a large range of initial propagators. Stable fixed points therefore lead to broadband excitation. (b) Points near an unstable fixed point diverge. Unstable fixed points may lead to narrowband excitation. In general, fixed points may be stable in some directions and unstable along other directions.

C. Simple mathematical example of fixed points

Before considering specific iterative schemes on propagators in Liouville space for NMR applications, i.e., mappings on the propagator space for spin systems, we review the properties of simple one- and two-dimensional functions, as an illustration of the significance of fixed points and their stability. This is basic and well known material[54,55] but it allows us to introduce some of the terminology and methods used in the later analysis. Consider first a function f of a single, real variable x. An example of such a function $f(x) = \frac{3}{2}x - x^3$ appears in Fig. 5. Beginning with any initial point x_0, f can be used to generate a series of iterates x_1, x_2, x_3, etc., with

$$x_n = f^n(x_0),$$

i.e., $x_0 \to x_1 \to x_2 \to x_3 \to \cdots$. The fixed points of f are those points $\bar{x}$ for which $\bar{x} = f(\bar{x})$. They can be found graphically as the points of intersection of the graph of f with a line through the origin with a slope of 1, i.e., $x_{n+1} = x_n$. In Fig. 5, the fixed points are $-\sqrt{1/2}$, 0, and $\sqrt{1/2}$.

The stability of $\bar{x}$ can be determined by evaluating the derivative of f at $\bar{x}$, i.e., $f'(\bar{x})$. In the neighborhood of $\bar{x}$,

$$f(x) = \bar{x} + f'(\bar{x})(x - \bar{x}) + O[(x - \bar{x})^2], \tag{4}$$

where $O[(x - \bar{x})^2]$ indicates a quantity on the order of $(x - \bar{x})^2$. The possible stability properties of $\bar{x}$ are summarized as follows:

$$\text{unstable: } |f'(\bar{x})| > 1, \tag{5a}$$

$$\text{stable: } 0 < |f'(\bar{x})| < 1, \tag{5b}$$

$$\text{superstable: } f'(\bar{x}) = 0. \tag{5c}$$

If $\bar{x}$ is stable, initial points near $\bar{x}$ converge to $\bar{x}$ geometrically, i.e.,

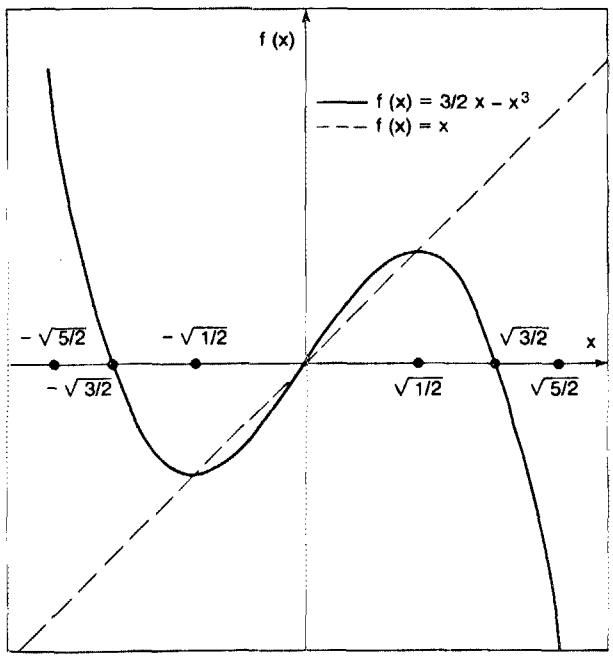

FIG. 5. A simple function of a single variable, with an unstable fixed point at 0 and stable fixed points at $\pm\sqrt{1/2}$. Except for isolated points, the entire open interval $(-\sqrt{5/2}, \sqrt{5/2})$ converges to $\pm\sqrt{1/2}$ with iterations of f. The isolated points map onto 0. Thus, stable fixed points dominate the dynamics of a function over a large range of initial points.

$$\lim_{n\to\infty} \frac{x_n - \bar{x}}{x_{n-1} - \bar{x}} = f'(\bar{x}). \tag{6}$$

The most rapid convergence occurs when $\bar{x}$ is superstable. Then points near $\bar{x}$ converge to within $O((x-\bar{x})^2)$ of $\bar{x}$ on a single iteration. In Fig. 5, the fixed points $\pm\sqrt{1/2}$ are superstable. The fixed point 0 is unstable, since $f'(0) = 3/2$.

The assessment of the stability of a fixed point is based on a linearization of the function in the neighborhood of the fixed point. Only the first derivative is considered, which is sufficient to characterize the behavior of a small interval of initial points except in marginal cases. However, when a fixed point is stable, it can affect the dynamics of the function far beyond its immediate neighborhood. Large regions of initial points, not only the nearby points, may converge to the fixed point. For example, all initial points in the open interval $(0,\sqrt{3/2})$ converge to the fixed point $\sqrt{1/2}$ in Fig. 5. All initial points in the interval $(-\sqrt{3/2},0)$ converge to $-\sqrt{1/2}$. In fact, it can be shown graphically[58,59] or numerically that all initial points in $(-\sqrt{5/2},\sqrt{5/2})$ converge to either $-\sqrt{1/2}$,0, or $\sqrt{1/2}$ upon iteration. The set of points that converge to a stable fixed point is called the *basin* of that fixed point.

The NMR examples in the following sections involve functions of more than one variable, because they act on a multidimensional propagator space. To demonstrate how to proceed in such a more complicated case, we generalize the function of Fig. 5 to the complex plane:

$$f(z) = \tfrac{3}{2}z - z^3. \tag{7}$$

If f is considered to be a function of two real variables x and y, with $z = x + iy$, Eq. (7) can be rewritten:

$$f\colon (x,y) \to (\tfrac{3}{2}x - x^3 + 3xy^2,\ \tfrac{3}{2}y + y^3 - 3x^2y). \tag{8}$$

f still has the same three fixed points on the real axis with coordinates $(\sqrt{1/2},0)$, $(0,0)$, and $(-\sqrt{1/2},0)$.

The stability of the fixed points of a function of many variables is determined by evaluating the Jacobian of the function at the fixed point, a natural generalization of the evaluation of the derivative in the one-dimensional case in Eq. (5). The Jacobian is a linear transformation, so that stability is again determined by a linearization of the function. If the eigenvalues of the Jacobian evaluated at a fixed point are all less than 1 in magnitude, the fixed point is stable. Otherwise, the fixed point is unstable but may have certain stable directions. If all eigenvalues are zero, the fixed point is superstable.

The Jacobian $J(x,y)$ of f in Eq. (8) is a 2×2 matrix given by

$$J(x,y) = \begin{pmatrix} 3/2 - 3x^2 + 3y^2 & 6xy \\ -6xy & 3/2 + 3y^2 - 3x^2 \end{pmatrix}. \tag{9}$$

Evaluated at the fixed points $(\pm\sqrt{1/2},0)$, J is the zero matrix. These fixed points are therefore superstable in the complex plane. At $(0,0)$, J is 3/2 time the unit matrix. $(0,0)$ is an unstable fixed point, with no stable directions.

D. Basin images

In the two-dimensional or complex case in Eqs. (7) and (8), we use a numerical procedure to determine the basins of the superstable fixed points. A portion of the complex plane is divided into a grid of small squares. The center of each square is chosen as an initial point. The iterates of each initial point are computed and checked for convergence to the desired fixed point. An iterate is considered to have converged if it is within a radius of 0.1 of the fixed point in the complex plane. Once convergence occurs, the iteration process stops and the number of iterations required for convergence is assigned to the square. If convergence does not occur within 15 iterations, the iteration process stops and the number -1 is assigned to the square. Finally, the selected portion of the complex plane is displayed on a graphics system, with each square shaded according to its assigned number. We call the resulting picture a *basin image*.

Figure 6 shows basin images for the two superstable fixed points of $f(z)$ in Eq. 7. The grid consists of squares with sides of length 0.02. Lighter shades correspond to smaller numbers, or more rapid convergence. Nonconvergent regions (-1) are filled with black. The symmetry of the basins for $(\sqrt{1/2},0)$ and $(-\sqrt{1/2},0)$ is a result of the fact that f is an odd function of z. The structure of the basins and the number of iterations required for the convergence of an initial point can be read directly from a basin image. From that information in Fig. 6, the dynamics of f can be inferred. For example, it is clear that there is a large, teardrop-shaped region around $(\sqrt{1/2},0)$ which converges to that fixed point. In addition, there is a smaller teardrop along the negative real axis that also converges to $(\sqrt{1/2},0)$. The similarity of shapes suggests that f maps the smaller teardrop onto the larger teardrop on the first iteration. The existence of other smaller and darker teardrops in the basin image indicates a succession of mappings of the small teardrops onto ever larger teardrops, leading to the eventual convergence.

Along with the concept of treating an iterative scheme as a function or mapping on the propagator space and the process of investigating fixed points and their stability, the examination of basin images is an important component of the fixed point theory as developed in subsequent sections. It gives a geometrical picture of how the iterative scheme works. In Sec. IV, we show how basin images can be used to guide the choice of the initial pulse sequence on which an iterative scheme acts. In addition, basin images reveal properties of iterative schemes that reflect the complexity and symmetry of the underlying dynamics, as will be seen in Secs. IV and VI.

E. Propagator space for a spin-1/2 or two-level system

Much of the development in subsequent sections deals with pulse sequences applied to isolated spins. The high field rotating frame Hamiltonian for an isolated spin during an rf pulse is always of the form

$$H = \Delta\omega I_z + \omega_1(I_x\cos\phi + I_y\sin\phi), \tag{10}$$

where ω_1 and ϕ are the rf field amplitude and phase, respectively, and $\Delta\omega$ is the resonance offset, or the difference

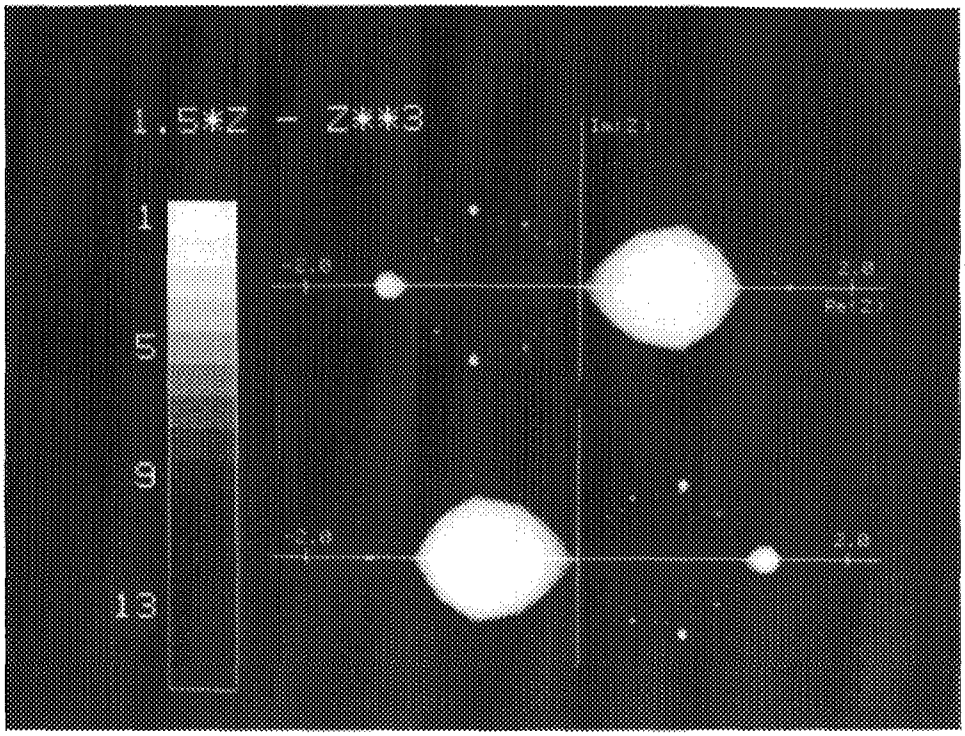

FIG. 6. Basin image for the complex function $f(z) = (3/2)z - z^3$ in the complex plane. A basin image reveals the set of initial points that converges to a fixed point, i.e., the basin of the fixed point, by shading regions according to the number of iterations required for convergence. Shown are the basins of the real fixed points $\sqrt{1/2}$ (top) and $-\sqrt{1/2}$ (bottom). A scale of shades corresponding to the number of iterations for convergence is shown to the left. The basins consist of multiple, disconnected regions with a self-similarity of structure.

between the rf frequency and the Larmor frequency. Equation (10) holds regardless of the total spin quantum number. In addition, Eq. (10) is the form of the Hamiltonian for any two-level, quantum mechanical system[60,61] if the spin angular momentum operators I_i are taken to be fictitious spin-1/2 operators.

If the pulse length is τ, the propagator for the pulse is

$$U(\tau) = \exp(-i\boldsymbol{\alpha} \cdot \mathbf{I}) \tag{11}$$

with

$$\boldsymbol{\alpha} = (\omega_1\tau \cos\phi, \omega_1\tau \sin\phi, \Delta\omega\tau). \tag{12}$$

The overall propagator for a pulse sequence is a product of operators in the form of Eq. (11), with $\boldsymbol{\alpha}$ varying from pulse to pulse or continuously as the rf amplitude, phase, and possibly frequency vary.

It is appropriate in NMR to describe the quantum statistical state of a spin system by a density operator, due to the fundamentally statistical nature of the ensemble being measured. For isolated spins or two-level systems, the density operator ρ is specified by a three-dimensional vector $\mathbf{M}$:

$$\rho = \mathbf{M} \cdot \mathbf{I}. \tag{13}$$

The effect of rf pulses in Eq. (11) is to rotate $\mathbf{M}$. Thus, in a density operator description, pulse sequence propagators are always rotations, with the rotation angle specified by $|\boldsymbol{\alpha}|$ and the rotation axis specified by the direction of $\boldsymbol{\alpha}$. Note again[7(a)] that we use the term propagator for what is in this case a superpropagator or Liouvillian since it transforms or propagates the density operator. The distinction is not critical for the discussions in this paper.

Any rotation in three-dimensional space can be represented by a 3×3 real, orthogonal matrix with a determinant of 1. Such matrices are the elements of a group, called $SO(3)$.[62] The elements of $SO(3)$ lie in the three-dimensional space of Fig. 7. The vector $\boldsymbol{\alpha}$ may be viewed as the coordinates of a rotation in that space. $SO(3)$ space is spherical, with a radius of π, since any product of rotations is equivalent to a net rotation of π or less about a single axis. In addition, antipodal points on the sphere are identified, since rotations by π about antiparallel axes are equivalent.

Points in $SO(3)$ in Fig. 7 along the x, y, or z axes represent rotations about the x, y, or z axes. The origin of $SO(3)$ represents a net rotation of zero, or the unit operator. Points on the equator of $SO(3)$ represent net rotations of π about axes in the xy plane. Such rotations correspond to the inversion of

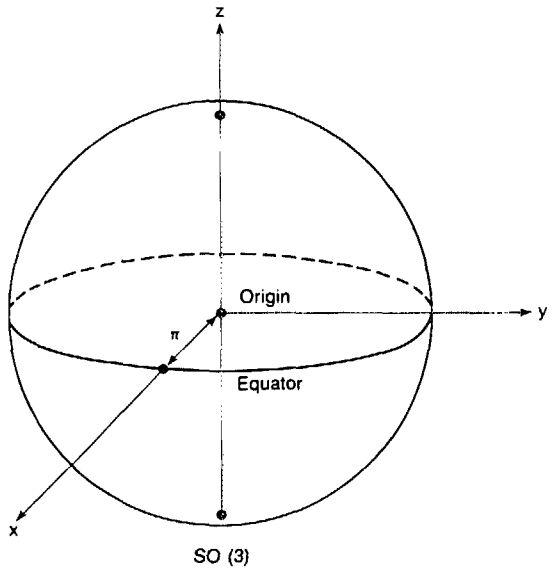

FIG. 7. $SO(3)$ space, the propagator space for pulse sequences applied to isolated spins or two-level spectroscopic systems. $SO(3)$ space is a sphere in three dimensions with a radius of π. Antipodal points are identified. A point in $SO(3)$ with coordinates $(\alpha_x, \alpha_y, \alpha_z) = \boldsymbol{\alpha}$ represents a rotation by $|\boldsymbol{\alpha}|$ about an axis along the direction of $\boldsymbol{\alpha}$. The equator represents π pulses, i.e., rotations that invert populations. The origin represents no net rotation, i.e., the unit operator.

spin state populations and therefore have a special significance in Secs. III–V below.

For isolated half-integral spins, the pulse sequence propagators form a group that is rigorously isomorphic to $SU(2)$, the group of unitary 2×2 matrices with a determinant of 1, rather than $SO(3)$.[63] Provided that a density operator description is employed, however, the distinctions between $SU(2)$ and $SO(3)$ become immaterial because the absolute phase of the fermion wave function is eliminated. We therefore take $SO(3)$ to be the propagator space for all isolated spin problems. This is consistent with the normal NMR picture of rf radiation rotating magnetization vectors about axes in the rotating frame.

III. FIXED POINT ANALYSIS OF ITERATIVE SCHEMES FOR POPULATION INVERSION

A. Definition and properties of phase shift schemes

There exist several iterative schemes which generate pulse sequences for broadband[1,5,6] or narrowband[1,6] population inversion. One class of schemes is pictured in Fig. 8 and defined as follows. Beginning with any initial pulse sequence S_0, we form N phase-shifted versions $S_0^{(i)}$ by applying overall rf phase shifts ϕ_i to S_0. For population inversion problems, N is required to be an odd integer. The first iterate sequence S_1 is then the concatenation of the phase-shifted versions of S_0 taken in order, i.e., $S_0^{(1)} S_0^{(2)} \cdots S_0^{(N)}$. The same phase shifts are applied to S_1, producing versions $S_1^{(i)}$ that are concatenated to form S_2. Repetitive application of the scheme generates higher iterate sequences. The sequence S_k is N^k times longer than S_0. We use the notation $[\phi_1,\phi_2,\ldots,\phi_N]$ to represent specific phase shift schemes, with the phase shifts given in degrees.

A phase shift scheme dictates a well-defined function F on $SO(3)$. In order to analyze that function, we use the notation $R(\alpha)$ to represent a point in $SO(3)$ corresponding to a rotation by $|\alpha|$ about an axis along the direction of α. $R_x(\epsilon)$ represents a rotation about the x axis by an angle ϵ, with analogous notation for rotations about the y and z axes. $R_\gamma(\epsilon)$ represents a rotation about an axis in the xy plane making an angle γ with the x axis. If the propagator for the sequence S_k is the point $R(\alpha)$ in $SO(3)$, then the propagator for $S_k^{(i)}$ is $R(\alpha_{\phi_i})$, with

$$\alpha_{\phi_i} = (\alpha_x \cos\phi_i - \alpha_y \sin\phi_i, \alpha_y \cos\phi_i + \alpha_x \sin\phi_i, \alpha_z). \tag{14}$$

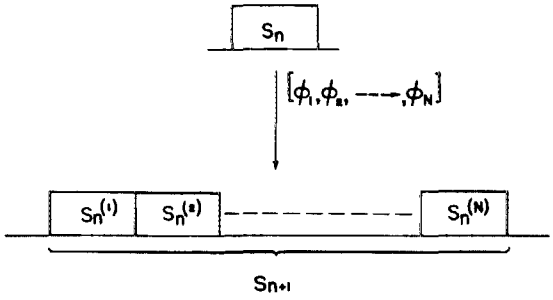

FIG. 8. Action of an iterative scheme based on phase shifts. The sequence S_{n+1} is generated from S_n by forming phase-shifted versions $S_n^{(k)}$, with phase shifts ϕ_k, and concatenating them. A phase shift scheme is depicted by the notation $[\phi_1, \phi_2,\ldots,\phi_N]$.

A phase shift merely rotates α about the z axis. The propagator for the sequence S_{k+1} is $R(\beta)$, given by

$$R(\beta) = R(\alpha_{\phi_N}) R(\alpha_{\phi_{N-1}}) \cdots R(\alpha_{\phi_1}). \tag{15}$$

Thus, F maps the point $R(\alpha)$ to the unique point $R(\beta)$.

F has certain fixed points that are immediately apparent. If $R(\alpha)$ is the unit operator, corresponding to a rotation of zero and the origin of $SO(3)$, then Eq. (15) shows that $R(\beta)$ is also the unit operator. The origin of $SO(3)$ in Fig. 7 is therefore always a fixed point.

If $R(\alpha)$ is $R_\gamma(\pi)$, that is, a rotation by π radians about an axis in the xy plane, then

$$R(\beta) = R_{\gamma+\phi_T}(\pi) \tag{16}$$

with

$$\phi_T = \phi_1 - \phi_2 + \cdots - \phi_{N-1} + \phi_N. \tag{17}$$

$R_\gamma(\pi)$ is a point on the equator of $SO(3)$. Equation (16) implies that the equator is in general an invariant set. Physically, this is apparent because $R_\gamma(\pi)$ is a rotation that inverts spin populations, transforming an initial density operator of I_z to $-I_z$. A phase-shifted version $R_{\gamma+\phi_i}(\pi)$ also inverts populations. Any product of an odd number of inverting rotations is itself another inverting rotation. ϕ_T is the net phase shift experienced by an inverting rotation. If the scheme is such that ϕ_T is a multiple of π, individual points on the equator of $SO(3)$ are fixed, recalling that antipodal points are identified.

The z axis of $SO(3)$ is also an invariant set. If $R(\alpha)$ is $R_z(\alpha)$, then $R(\beta)$ is $R_z(N\alpha)$. In addition to the origin, the other points along the z axis that are individually fixed are those that satisfy $\alpha = 2n\pi/(N-1)$.

B. Stability of fixed points

1. The origin

The stability of the origin of $SO(3)$, corresponding to the unit propagator, plays an important role in the dynamics of iterative schemes for narrowband population inversion and heteronuclear decoupling, discussed in Secs. V and VI. If the origin is stable, pulse sequences that produce no net rotation may be generated. To determine the stability of the origin under a general scheme of the form $[\phi_1,\phi_2,\ldots,\phi_N]$, we linearize Eq. (15) about the origin. This is conveniently done by evaluating the right-hand side of Eq. (15) to first order in $|\alpha|$. The result is

$$\beta = \alpha_{\phi_N} + \alpha_{\phi_{N-1}} \cdots + \alpha_{\phi_1}. \tag{18}$$

Equation (18) expresses F as a linear transformation $T^{(\text{origin})}$ on the vector α near the origin:

$$\beta = T^{(\text{origin})}\alpha \tag{19}$$

$$T^{(\text{origin})} = \begin{pmatrix} \sum_{n=1}^{N} \cos\phi_n & \sum_{n=1}^{N} \sin\phi_n & 0 \\ -\sum_{n=1}^{N} \sin\phi_n & \sum_{n=1}^{N} \cos\phi_n & 0 \\ 0 & 0 & N \end{pmatrix}. \tag{20}$$

One eigenvector of $T^{(\text{origin})}$ is (0,0,1), a vector along the z axis. The corresponding eigenvalue is N. Since $N>1$, the z axis of $SO(3)$ is always an unstable direction. The other eigenvectors

are $(1,i,0)$ and $(1,-i,0)$, with eigenvalues λ_0^+ and λ_0^-, respectively:

$$\lambda_0^{\pm} = \sum_{n=1}^{N} \exp(\pm i\phi_n). \tag{21}$$

The existence of complex eigenvectors and eigenvalues is indicative of a rotation. $T^{(\text{origin})}$ stretches or shrinks vectors in the xy plane by a factor of $|\lambda_0^+|$ and rotates them about z by an angle ϕ_+, where ϕ_+ is the phase of λ_0^+. The stability of the origin of $SO(3)$ along directions in the xy plane is thus determined by $|\lambda_0^+|$. If $\lambda_0^{\pm} < 1$, the origin is stable with respect to displacements in the xy plane. Equation (21) implies

$$|\lambda_0^+| = \left[\left(\sum_{n=1}^{N} \cos\phi_n\right)^2 + \left(\sum_{n=1}^{N} \sin\phi\right)^2\right]^{1/2}. \tag{22}$$

2. The equator

The stability of the equator (rotations by π around axes in the xy plane) plays an essential part in the dynamics of iterative schemes for broadband and narrowband population inversion. As will be seen, a stable equator leads to broadband inversion sequences. An unstable equator, combined with a stable origin, leads to narrowband inversion sequences. A linearization of F about the equator of $SO(3)$ may be carried out using the following general form for a rotation operator:

$$R(\alpha) = R_\gamma(\pi)R(\epsilon) \tag{23}$$

with

$$\epsilon = (\epsilon_x,\epsilon_y,0). \tag{24}$$

Equation (23) expresses an arbitrary rotation as the product of two rotations about axes in the xy plane, the first by $|\epsilon|$ and the second by π. If the net rotation is nearly an inverting rotation, $R(\epsilon)$ is a small, error rotation. Appendix A contains a proof of the generality of Eq. (23).

Reference 1 contains a derivation of the linearization of F about the equator based on the form in Eq. (23). Using Eq. (23), Eq. (15) becomes

$$R(\beta) = R_{\gamma+\phi_N}(\pi)R(\epsilon_{\phi_N})R_{\gamma+\phi_{N-1}}(\pi) \times R(\epsilon_{\phi_{N-1}})\cdots R_{\gamma+\phi_1}(\pi)R(\epsilon_{\phi_1}). \tag{25}$$

With the aid of the following identities:

$$R_\phi(\pi) = R_x(\pi)R_z(-2\phi), \tag{26}$$

$$R(\epsilon_\phi) = R_z(\phi)R(\epsilon)R_z(-\phi), \tag{27}$$

$$R_x(\pi)R(\epsilon)R_x(-\pi) = R(\bar{\epsilon}), \tag{28}$$

where

$$\bar{\epsilon} = (\epsilon_x, -\epsilon_y, 0), \tag{29}$$

we evaluate Eq. (25) to first order in $|\epsilon|$ as

$$R(\beta) = R_{\gamma+\phi_T}(\pi)R(\epsilon_T), \tag{30}$$

where

$$\epsilon_T = \sum_{n=1}^{N} (\epsilon_x \cos\Gamma_n - \epsilon_y \sin\Gamma_n, (-1)^{n+1}\epsilon_y \cos\Gamma_n + (-1)^{n+1}\epsilon_x \sin\Gamma_n, 0), \tag{31}$$

$$\Gamma_n = \begin{cases} \phi_n + \sum_{m=1}^{n-1} (-1)^{m+1} 2\phi_m, & n \text{ odd} \\ \phi_n - 2\gamma + \sum_{m=1}^{n-1} (-1)^m 2\phi_m, & n \text{ even} \end{cases}. \tag{32}$$

Equation (31) presents F as a linear transformation acting on ϵ in the neighborhood of the equator. However, in studying the mapping of $R(\alpha)$ to $R(\beta)$, we must take into account the phase shift ϕ_T. It is the direction of ϵ relative to the phase γ and the direction of ϵ_T relative to the phase $\gamma + \phi_T$ that are important in determining the extent of population inversion. The actual value of the phase is unimportant, and is defined arbitrarily. For this reason, we remove the phase shift ϕ_T by rewriting Eq. (30) as

$$R(\beta) = R_z(\phi_T)R_\gamma(\pi)R(\epsilon'_T)Rz(-\phi_T), \tag{33}$$

where

$$\epsilon'_T = \sum_{n=1}^{N} (\epsilon_x \cos\Gamma'_n - \epsilon_y \sin\Gamma'_n, (-1)^{n+1}\epsilon_y \cos\Gamma'_n + (-1)^{n+1}\epsilon_x \sin\Gamma'_n, 0), \tag{34}$$

$$\Gamma'_n = \Gamma_n + (-1)^n\phi_T. \tag{35}$$

The linear transformation in Eq. (34) is expressed in matrix form, in the $\{x,y\}$ basis, as

$$\epsilon'_T = T^{(\text{equator})}\epsilon, \tag{36}$$

$$T^{(\text{equator})} = \begin{pmatrix} \sum_{n=1}^{N} \cos\Gamma'_n & -\sum_{n=1}^{N} \sin\Gamma'_n \\ \sum_{n=1}^{N} (-1)^{n+1} \sin\Gamma'_n & \sum_{n=1}^{N} (-1)^{n+1} \cos\Gamma'_n \end{pmatrix}. \tag{37}$$

The fact that $T^{(\text{equator})}$ is a 2×2 matrix reflects the fact that there are only two directions for displacements from the equator. The eigenvectors and eigenvalues of $T^{(\text{equator})}$ depend on the choice of the rf phase shifts ϕ_i in the iterative scheme. For example, an iterative scheme with a stable equator is derived by choosing the ϕ_i such that the eigenvalues of $T^{(\text{equator})}$ are both less than 1 in magnitude. Three possible scenarios exist. First, the eigenvalues can be real and distinct, implying the existence of two real eigenvectors. Second, the two eigenvalues can be complex and conjugate to one another, implying two complex conjugate eigenvectors. Third, the two eigenvalues can be real and degenerate. In this case, there may be either one or two independent real eigenvectors. The linearization of the function corresponding to an iterative scheme is generally not Hermitian, and so need not have a complete basis of eigenvectors. The eigenvalues of $T^{(\text{equator})}$ are $\lambda_e^{\pm}$, given by

$$\lambda_e^{\pm} = (\cos\Gamma'_1 + \cos\Gamma'_3 + \cdots + \cos\Gamma'_N) \pm [(\cos\Gamma'_2 + \cos\Gamma'_4 + \cdots + \cos\Gamma'_{N-1})^2 + (\sin\Gamma'_2 + \sin\Gamma'_4 + \cdots + \sin\Gamma'_{N-1})^2 - (\sin\Gamma'_1 + \sin\Gamma'_3 + \cdots + \sin\Gamma'_N)^2]^{1/2}. \tag{38}$$

The eigenvalues are independent of γ. The eigenvectors for $\gamma \neq 0$ are related to those for $\gamma = 0$ by rotation about z by γ.

IV. GENERATION OF SEQUENCES FOR BROADBAND POPULATION INVERSION

A. Derivation of schemes using vector diagrams

Pulse sequences that invert spin populations over large ranges of the resonance offset $\Delta\omega$ and the rf amplitude ω_1 can be generated by iterative schemes for which the equator of $SO(3)$ is stable and the origin is unstable, as in Fig. 9. Such schemes can be found by searching for a combination of phase shifts for which $|\lambda_e^{\pm}| < 1$ in Eq. (38). An alternative method, which is particularly useful for assuring superstability, is to use vector diagrams, as in Fig. 10. Equation (34) implies that ϵ_T' is the sum of N vectors with equal magnitudes in the xy plane. These vectors may be divided into two groups, those with odd n and those with even n. Those with odd n are rotated about z by Γ_n'. Those with even n, in addition to being rotated about z by Γ_n', are rotated about x by π. If $\{\Gamma_n'\}$ can be found such that the two groups of vectors separately add up to zero, ϵ_T' will be zero regardless of ϵ and regardless of γ. In other words, $T^{(\text{equator})}$ in Eq. (37) is the zero matrix. The equator of $SO(3)$ is then superstable. Note that a minimum N of 5 is required. For $N = 5$, possible superstability conditions are

$$\Gamma_3 = \Gamma_1 + 2\pi/3, \tag{39a}$$

$$\Gamma_4 = \Gamma_2 + \pi, \tag{39b}$$

$$\Gamma_5 = \Gamma_1 + 4\pi/3. \tag{39c}$$

The phase shifts ϕ_n may be determined from Γ_n with Eq. (32). Two schemes that satisfy Eq. (39) are [0,0,120,60,120] and [0,330,60,330,0], as proposed in Ref. 1. For later comparison, plots of the extent of population inversion as a function of the relative resonance offset $\Delta\omega/\omega_1^0$ for pulse sequences generated by [0,0,120,60,120] are shown in Fig. 11. ω_1^0 is the nominal rf amplitude, used to define pulse lengths. The sequences in Fig. 11 were generated using a single π pulse as the initial sequence. When $\Delta\omega = 0$ and $\omega_1 = \omega_1^0$, a π pulse produces complete population inversion, corresponding to a propagator on the equator of $SO(3)$. Since the equator of $SO(3)$ is superstable under [0,0,120,60,120], initial points converge to the equator from all directions. Thus, the sequences generated by [0,0,120,60,120] produce broadband population inversion with respect to all experimental parameters that affect the propagator, i.e., both ω_1 and $\Delta\omega$.[1]

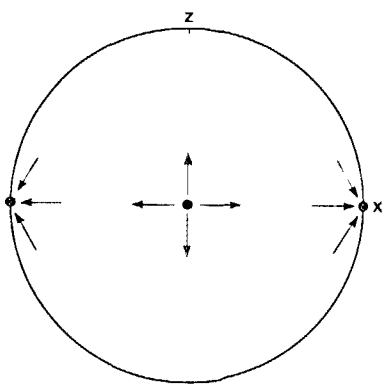

FIG. 9. The essential dynamical properties of phase shift schemes which generate pulse sequences for broadband population inversion. Shown is the xz plane of $SO(3)$. The origin is an unstable fixed point. The equator is a stable invariant set. Points in $SO(3)$ may converge to the equator, i.e., to inverting (π) rotations under iteration.

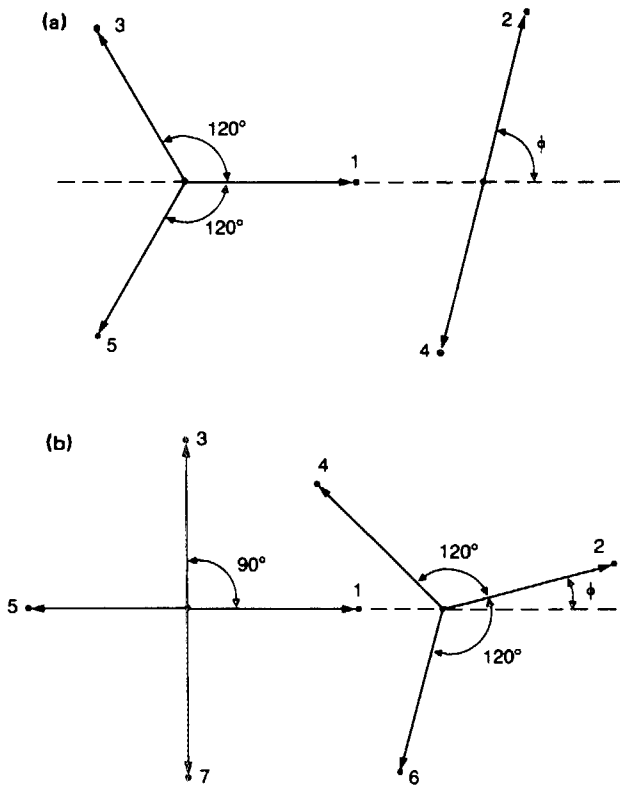

FIG. 10. Vector diagrams for deriving phase shift schemes for which the equator of $SO(3)$ is superstable. (a) Diagram for five-phase schemes of the form $[0,\phi,120+2\phi,60+3\phi,120+4\phi]$. (b) Diagram for seven-phase schemes of the form $[0,\phi,90+2\phi,300+3\phi,240+4\phi,300+5\phi,90+6\phi]$. The mutual cancellation of the vectors ensures superstability.

B. Construction of basin images

Figure 11 reveals several striking features. The sequences generated by [0,0,120,60,120] invert populations essentially perfectly over a very large range of offsets around zero, approximately $-1 < \Delta\omega/\omega_1^0 < 1$. In addition, there are other smaller ranges of offsets over which population

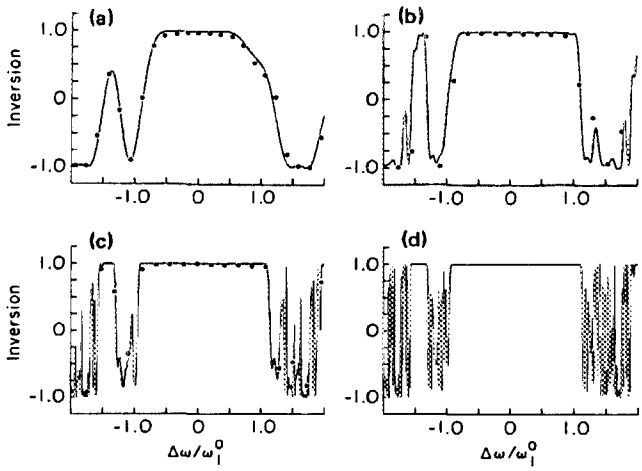

FIG. 11. Population inversion performance of the first four iterate sequences generated from an initial single π pulse by the scheme [0,0,120,60,120] [(a)–(d), respectively] as a function of the relative resonance offset. An inversion value of 1.0 represents complete population inversion; a value of -1.0 represents equilibrium populations. Dots are experimental measurements, from ^{1}H NMR of a $H_2O_{(l)}$ sample. Lines are simulations. Note that offset ranges of nearly complete inversion develop, separated by ranges of wildly varying inversion.

inversion is also achieved. In between, there are ranges of offsets over which the inversion varies chaotically. Qualitatively similar features appear in plots of the inversion as a function of relative rf amplitudes ω_1/ω_1^0. These features are reminiscent of the structure of the basin of a stable fixed point, as described in Sec. II and Fig. 6. Therefore, we examine the basin of the equator of $SO(3)$ under the mapping corresponding to [0,0,120,60,120] using basin images as introduced in Sec. II. In particular, we seek to answer the following questions:

1. What limits the inversion bandwidths in Fig. 11?

2. Why are there separated regions of complete inversion?

3. Why are there regions of chaotic fluctuations of the inversion?

The numerical construction of basin images for iterative schemes follows the procedure that led to Fig. 6. A grid of initial points in $SO(3)$ is selected. For each initial point, the corresponding 3×3 rotation matrix $R(\alpha)$ is set up. Phase-shifted versions $R(\alpha_\phi)$ are constructed according to Eq. (27) and multiplied together according to Eq. (15), resulting in the 3×3 matrix corresponding to the first iterate point. Continuing in this way, higher iterates are generated. Each iterate is checked for convergence to the form $R_\gamma(\pi)$. The criterion for convergence is

$$[R(\alpha)]_{zz} < -0.998. \tag{40}$$

where $[R(\alpha)]_{zz}$ is the matrix element of $R(\alpha)$ in the $\{x,y,z\}$ basis that represents the projection onto the z axis of a unit vector, initially aligned with $+z$, after rotation by $R(\alpha)$. The number of iterations required for convergence is assigned to each initial point. The number -1 is assigned to those points that do not converge within 15 iterations.

The construction of a basin image is greatly simplified by symmetry with respect to rotations about the z axis. For any $[\phi_1,\phi_2,\ldots,\phi_N]$ scheme, if two initial points are related by a rotation about z by some angle, then their iterates are related by the same rotation. This is a consequence of Eq. (15). The two initial points necessarily converge in the same number of iterations. Therefore, it is sufficient to consider a single cross section of $SO(3)$ containing the z axis.

Figure 12 is a basin image for [0,0,120,60,120], displayed on a graphics system in the manner of Fig. 6. It is clear that the basin of the equator of $SO(3)$ is nearly the entire space. However, embedded in $SO(3)$ there is a set of points that apparently does not converge to the equator. The basin has a repeating structure that is the consequence of the mapping of smaller basin regions onto larger ones as described in Sec. II C. The basin image, as a visualization of the dynamics of [0,0,120,60,120], provides an explanation of the features seen in Fig. 11. If the value of the parameter $\Delta\omega$ is such that the initial propagator lies in a convergent region of $SO(3)$, spins with that value of $\Delta\omega$ will be nearly completely inverted by a high iterate sequence. The fact that there are disconnected convergent regions implies that there may be disconnected ranges of $\Delta\omega$ for which the inversion becomes complete. The limits on the inversion bandwidth are established by values of $\Delta\omega$ for which the initial propagator belongs to the nonconvergent set.

The nonconvergent set in Fig. 12 has an intricate, filamentous structure. It is likely that there are convergent "holes" in the nonconvergent set occurring at all levels of magnification. In that case, the nonconvergent set is a fractal[64] surface in $SO(3)$, with a dimension between two and three. This fractal surface gives rise to the chaotic variations in the inversion for some ranges of $\Delta\omega$ in Fig. 11.

Figure 13 is a basin image for [0,330,60,330,0]. The qualitative features of Fig. 12 are reproduced, namely the existence of disconnected convergent regions separated by fractal, nonconvergent set of points. In addition, there is symmetry with respect to reflections in the xy plane. This is the result of the symmetry of the phase shifts, namely,

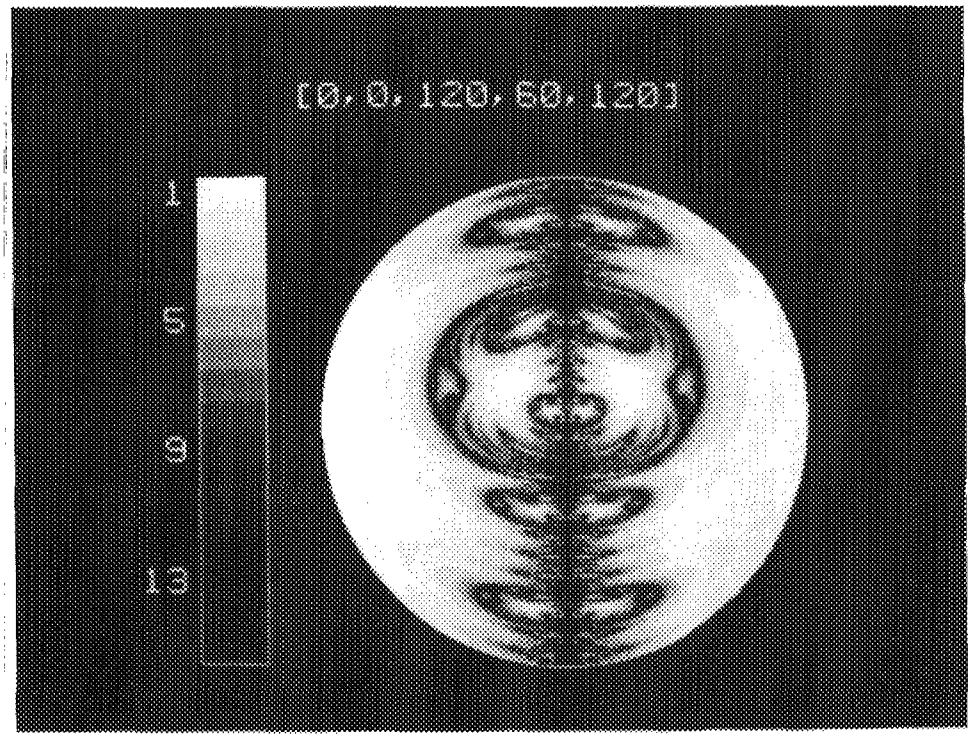

FIG. 12. Basin image for the iterative scheme [0,0,120,60,120]. Shown is a cross section through $SO(3)$, containing the z axis. Convergence to the equator is displayed. Lighter shades correspond to more rapid convergence. The basin of the equator is nearly the entire space. Points that do not converge to the equator, depicted in black, apparently form a fractal set.

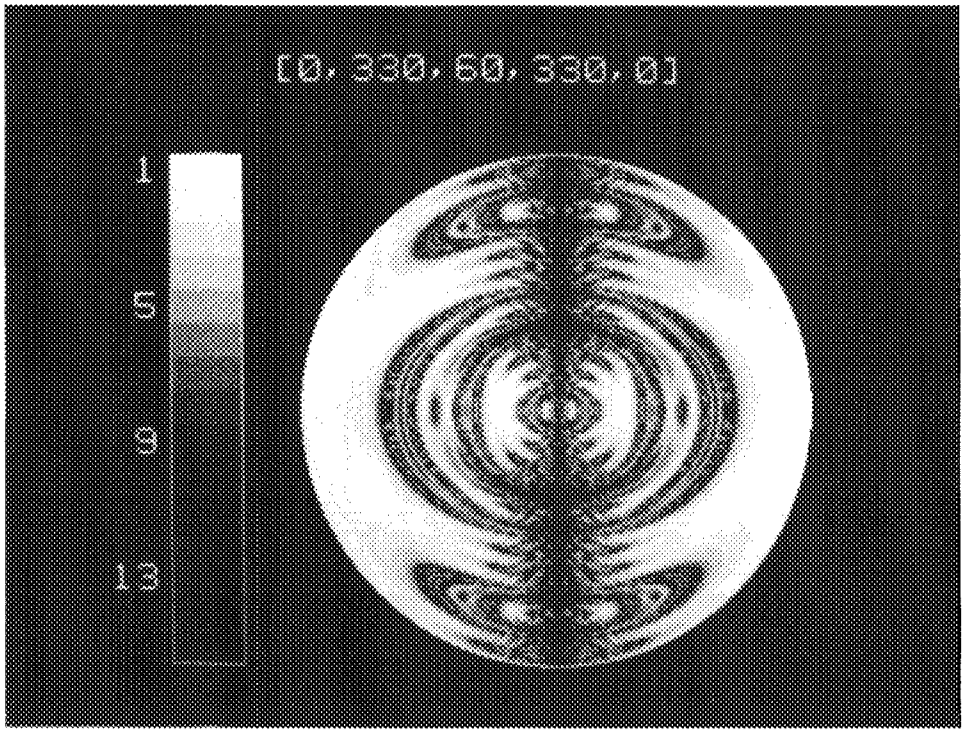

FIG. 13. Basin image for the scheme [0,330,60,330,0]. Qualitative features are similar to the basin image for [0,0,120,60,120] shown in Fig. 12. The additional reflection symmetry in this figure arises from the symmetry of the phase shifts.

$$\phi_{N-i} = \phi_{i+1}. \tag{41}$$

It is shown in Appendix B that Eq. (41) implies that, if two initial points are related by reflection in the xy plane, their iterates must also be related by reflection. Therefore, the two points must converge in the same number of iterations.

C. Optimization of the initial pulse sequence

Basin images such as those in Figs. 12 and 13 can be used to guide the selection of an initial pulse sequence. An initial pulse sequence is specified by a sequence of flip angles and rf phases. The flip angle of the ith pulse in the sequence is $\omega_1^0 \tau_i$ where τ_i is the length of the pulse. When $\Delta\omega = 0$ and $\omega_1 = \omega_1^0$, the initial sequence produces a net rotation that is a single point in $SO(3)$. However, there are always experimental variations of $\Delta\omega$ and ω_1 that produce variations in the net rotation, so that the initial sequence actually corresponds to a locus of points in $SO(3)$. In the most general terms, an initial pulse sequence corresponds to a locus of points in the propagator space, dictated by the nominal flip angles and phases and by the experimentally relevant ranges of parameters in the Hamiltonian.

As an example, Fig. 14 shows the loci of points in $SO(3)$ corresponding to a single π pulse with separate variations of ω_1 and $\Delta\omega$. The inversion plots in Fig. 11 could be predicted by comparing Fig. 14(b) with Fig. 12. The ranges of offsets where the inversion is nearly complete in Fig. 11 are the segments of the locus in Fig. 14(b) that lie on top of the rapidly convergent regions in Fig. 12.

For broadband excitation problems in general, the range of parameters over which an iterative scheme is effective can be enlarged by choosing an initial sequence for which the locus of initial points conforms to the basin of the desired fixed point. This is illustrated schematically in Fig. 15. For the case of the scheme [0,0,120,60,120], the largest part of the basin is roughly defined by the requirements

$$40° \leqslant \phi \leqslant 140°, \tag{42a}$$

$$0.70\pi \leqslant r \leqslant \pi \tag{42b}$$

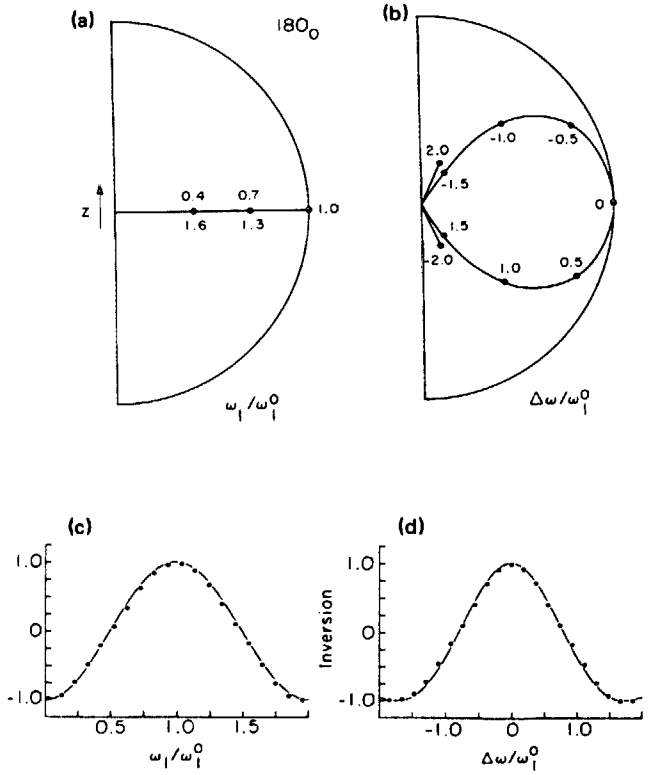

FIG. 14. Loci of points in $SO(3)$ corresponding to a single π pulse with variations in the rf amplitude (a) or the resonance offset (b) and the corresponding inversion profiles for I_z in (c) and (d). Shown in (a) and (b) is half of the xz plane of $SO(3)$. The points are rotated about z so that they lie in the pictured plane. Comparison of these loci of points with the basin images in Figs. 12 and 13 reveals the ranges of rf amplitudes and resonance offsets over which complete population inversion may be achieved by applying the schemes [0,0,120,60,120] and [0,330,60,330,0] to an initial single π pulse.

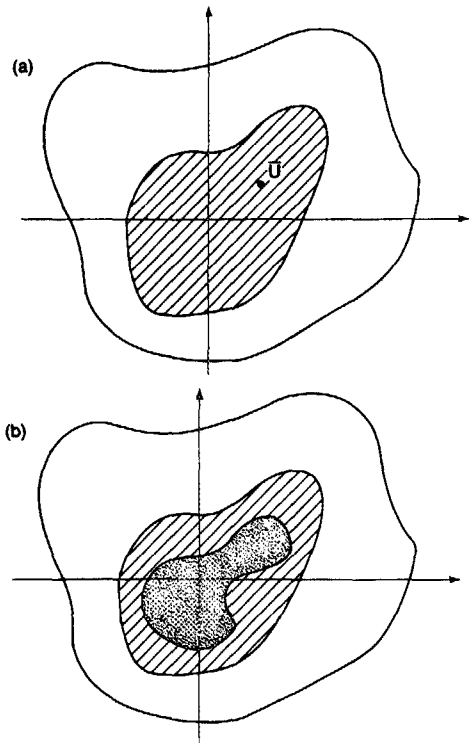

FIG. 15. Illustration of the principle of matching the initial locus of points to the basin in order to optimize the exictation bandwidth produced by an iterative scheme. (a) A stable fixed point $\bar{U}$ is shown in an abstract propagator space. The basin of $\bar{U}$ is filled with diagonal lines. (b) An initial pulse sequence is chosen so that the corresponding locus of initial points in the propagator space, arising from variations in experimental parameters and depicted as the shaded region, lies inside the basin. It is then guaranteed that the propagator for the iterate sequence will converge to $\bar{U}$ over the entire range of experimental parameters. Note that the locus of initial points need not be concentrated near $\bar{U}$.

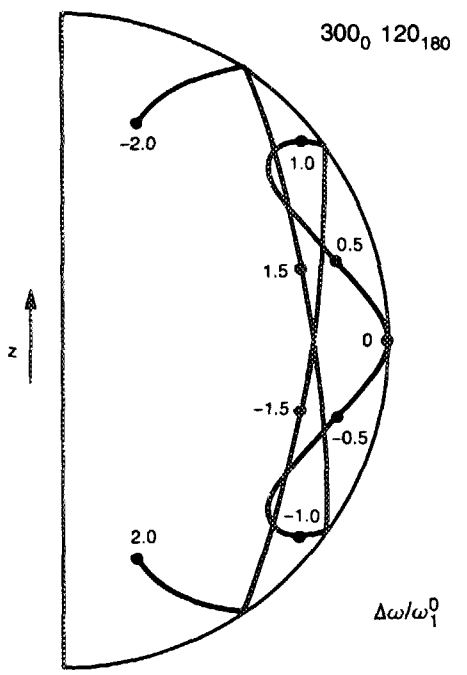

FIG. 16. Locus of points in $SO(3)$ corresponding to the sequence 300_0120_{180} with variations in the resonance offset. Initial points are rotated about z so as to lie in the xz plane. 300_0120_{180} is chosen to conform to the basin of the equator of $SO(3)$ under the scheme [0,0,120,60,120], shown in Fig. 12.

where ϕ and r are polar coordinates in $SO(3)$. An initial sequence for which the locus of points satisfies Eq. (42) for $-1.4\,\omega_1^0 < \Delta\omega < 1.4\,\omega_1^0$ is the sequence 300_0120_{180}, using the standard notation θ_γ for a pulse with a flip angle θ and a phase γ. The locus of points for 300_0120_{180} with variations in $\Delta\omega$ is shown in Fig. 16. The locus in Fig. 16 clearly conforms to the basin in Fig. 12. Figure 17 shows inversion plots for iterate sequences generated from 300_0120_{180} by [0,0,120,60,120]. The range of offset values for which the inversion is nearly complete is approximately twice as large as that in Fig. 11. Note that it is not essential that the initial sequence itself produce broadband inversion, but only that it conform to the basin.

To find the sequence 300_0120_{180}, a computer search was conducted over possible sequences consisting of two pulses with phases of 0° and 180° and flip angles in increments of 10°. For each possible sequence, the points in $SO(3)$ are calculated for values of $\Delta\omega$ between $-1.4\,\omega_1^0$ and $1.4\,\omega_1^0$, in increments of $0.1\,\omega_1^0$. This is done by treating the pulse sequence as a product of 3×3 rotation matrices. By examining the matrix elements of the net rotation $R(\alpha)$, the vector α that specifies the coordinates of the point in $SO(3)$ can be extracted.

As a second example of the selection of an initial sequence to improve the performance of an iterative scheme, consider the generation of sequences for simultaneous broadband inversion with respect to $\Delta\omega$ and ω_1 by the scheme [0,330,60,330,0]. Figure 18(a) shows the locus of points for a single π pulse with simultaneous variations in $\Delta\omega$ and ω_1. Figure 18(b) shows the locus for the sequence $165_0165_{105}165_0$ with the same variations in $\Delta\omega$ and ω_1. $165_0165_{105}165_0$ is chosen to conform to the basin of [0,330,60,330,0] in Fig. 13, using a search procedure as outlined above. Figure 19 shows inversion coutour plots for sequences generated from a single π pulse and from $165_0165_{105}165_0$ by [0,330,60,330,0]. The area for which the inversion is nearly complete is enlarged by the choice of an initial sequence that conforms to the basin.

Thus, the basin images provide not only an explanation of the performance of the broadband inversion schemes, but also a prescription for optimizing the performance. The principal of matching the initial sequence to the basin may be applied to broadband excitation problems in general.

V. GENERATION OF SEQUENCES FOR NARROWBAND POPULATION INVERSION

A. Derivation and performance of schemes

In Ref. 1, the scheme [0,120,240] was proposed for the problem of narrowband population inversion, in particular, narrowband with respect to the rf amplitude. For [0,120,140], the eigenvalues of $T^{(\text{origin})}$ and $T^{(\text{equator})}$, the linearizations of F at the origin and the equator, are respectively $\lambda_0^{\pm} = 0$ and $\lambda_e^{\pm} = -1 \pm \sqrt{2}i$. The origin of $SO(3)$ is superstable with respect to displacements in the xy plane; the equator is unstable. This is illustrated in Fig. 20. If the initial sequence is a single π pulse, the perfect inversion at $\omega_1 = \omega_1^0$ is preserved upon iteration. However, initial points near the equator, arising from rf amplitudes somewhat greater than

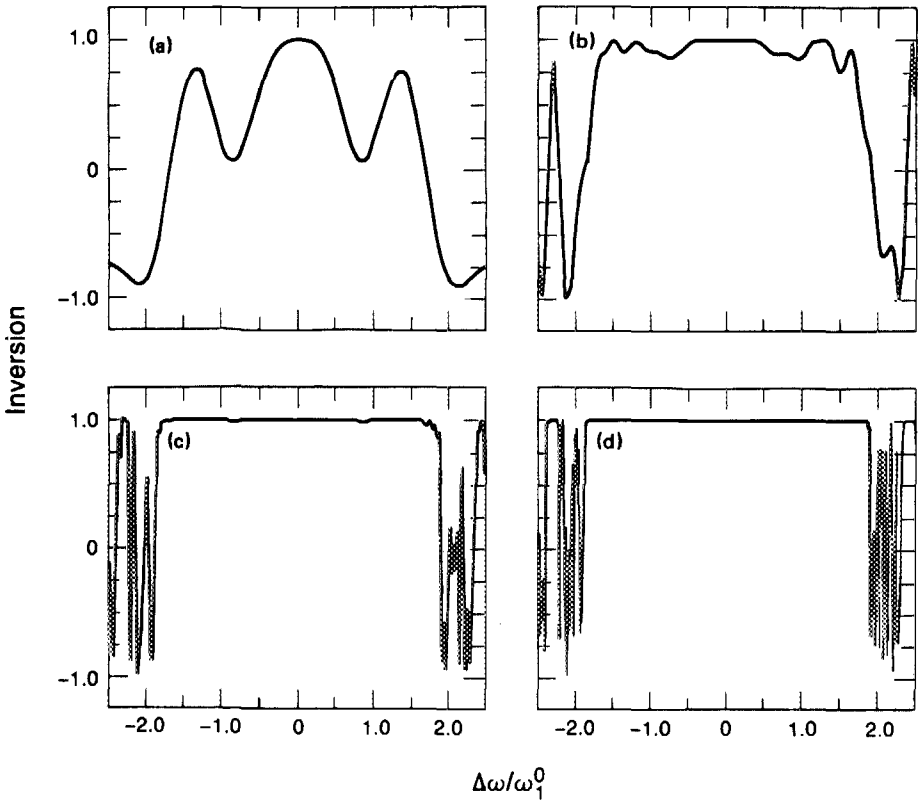

FIG. 17. Simulations of population inversion as a function of the resonance offset for the sequence 300_0120_{180} (a) and its first three iterates (b), (c), (d) generated by [0,0,120,60,120]. Compared to Fig. 11, the inversion bandwidths of the high iterate sequences are nearly doubled by choosing an initial sequence whose locus of points in *SO* (3) conforms to the basin of the equator.

or less than ω_1^0, are repelled from the equator. Initial points near the origin, arising from rf amplitudes near 0 or $2\omega_1^0$, move towards the origin. The result is the development of a narrow region of population inversion centered around $\omega_1 = \omega_1^0$. Inversion plots for sequences generated by [0,120,240] are shown in Fig. 21, for the sake of comparison.

Schemes for which the origin is superstable with respect to displacements in the xy plane can be derived with vector diagrams, as were the schemes in Sec. IV. Equation (18) implies that the origin is superstable in the xy plane for the scheme $[\phi_1,\phi_2,\cdots,\phi_N]$ if N unit vectors in the xy plane at angles ϕ_i to the x axis add up to zero.

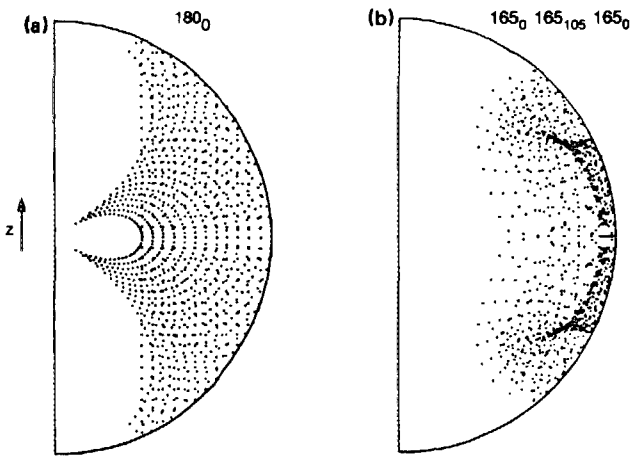

FIG. 18. Loci of points in *SO* (3) for the single pulse 180_0 (a) and the pulse sequence $165_0165_{105}165_0$ (b) resulting from simultaneous variations of the resonance offset and the rf amplitude. Points for offsets in the range $-1.0<\Delta\omega/\omega_1^0<1.0$ in increments of 0.05 and rf amplitudes in the range $0.4<\omega_1/\omega_1^0<1.6$ in increments of 0.05 are plotted. The points are rotated about z so as to lie in the xz plane. $165_0165_{105}165_0$ is chosen to conform to the basin of the equator of *SO* (3) under [0,330,60,330,0], shown in Fig. 13.

As is apparent in Fig. 21(d), the narrowband inversion profile is only a transient result of the scheme [0,120,240]. An explanation of this feature is provided by Fig. 22, which shows the movement of representative initial points under [0,120,240]. Because the origin of *SO* (3) is unstable along the z axis, initial points in the xy plane move toward the origin on the lower iterations but then diverge from the origin along the z axis. Thus, significant inversion develops at intermediate values of ω_1 on higher iterations.

The escape of points from the xy plane can be prevented by using a scheme with symmetric phase shifts in the sense of Eq. (41). The reflection symmetry discussed in Sec. IV B and Appendix B constrains initial points in the xy plane to remain in the xy plane. An example of a scheme with the desired symmetry is $[180\text{-}\cos^{-1}0.25,\ 180+\cos^{-1}0.25,\ 0,\ 180+\cos^{-1}0.25,\ 180-\cos^{-1}0.25]$, or approximately [104.5, 255.5, 0, 255.5, 104.5]. For this scheme, $\lambda_0^{\pm}=0$ and $\lambda_e^{\pm}=2.375\pm0.5$. Initial points in the xy plane move from the equator to the origin upon iteration. Inversion plots as a function of ω_1 for sequences generated from an initial single π pulse are shown in Fig. 23. The narrowband inversion profile is clearly not transient. Rather, the inversion bandwidth decreases indefinitely with increasing iterations.

B. Resonance offset behavior

Pulse sequences for narrowband population inversion with respect to the rf amplitude, generated by schemes such as [0,120,240] and [104.5,255.5,0,255.5,104.5], typically exhibit inversion plots as a function of the resonance offset that resemble those in Fig. 24. A possible application of the narrowband sequences is the spatial localization of NMR sig-

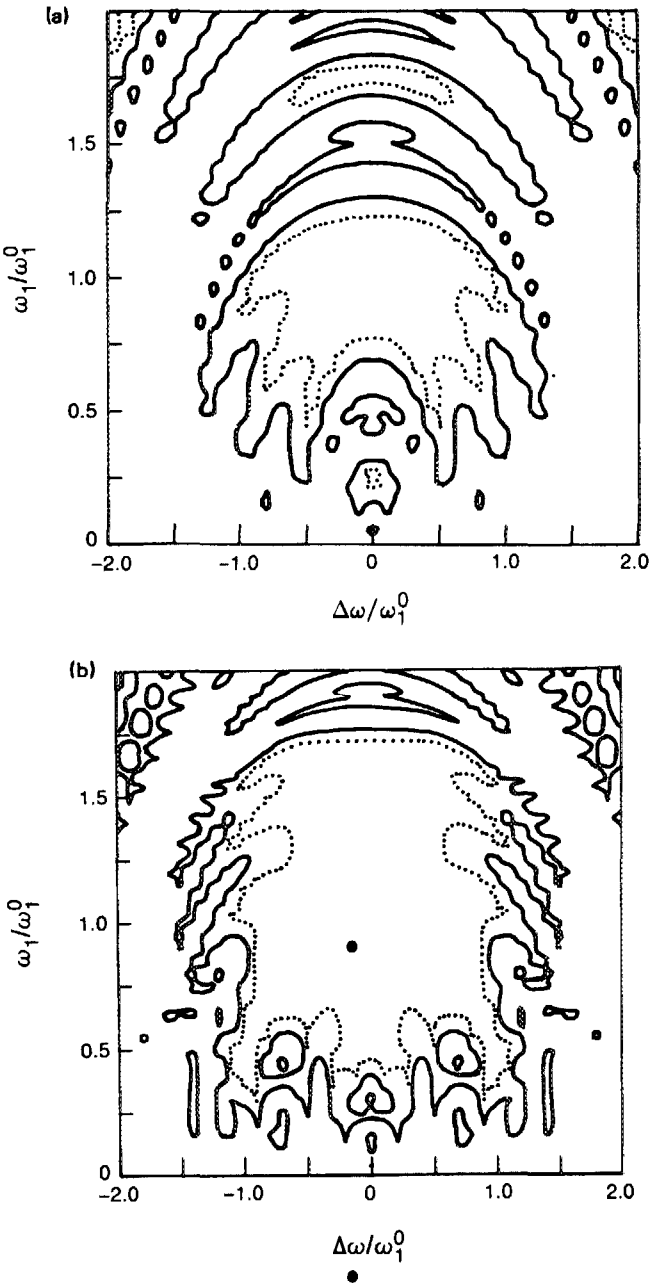

FIG. 19. Calculated inversion contour plots for pulse sequences which are the second iterates of 180_0 (a) and $165_0165_{105}165_0$ (b) under [0,330,60,330,0]. Shown are the 0.99 (dotted lines) and 0.50 (solid lines) inversion contours. The area of nearly complete population inversion is enlarged by choosing an initial sequence for which the locus of points in $SO(3)$ conforms to the basin of the equator for simultaneous variations of the resonance offset and the rf amplitude.

nals in rf field gradients.[6,20–22] In such an application, the sensitivity to resonance offset apparent in Fig. 24 severely limits the frequency range over which signals can be uniformly localized. Pulse sequences that invert spin populations over a narrow range of rf amplitudes but over a broad range of resonance offsets are needed.

As a step towards the derivation of such narrowband–broadband combination sequences, we examine iterative schemes with stability properties illustrated by Fig. 25. Consider the scheme [0,200,230,30,95]. For this scheme, $\lambda_0^{\pm} = 0.196 \pm 0.388i$ so that the origin is stable in the xy plane. According to Eq. (37), with $\gamma = 0$, the linear transformation at the equator is

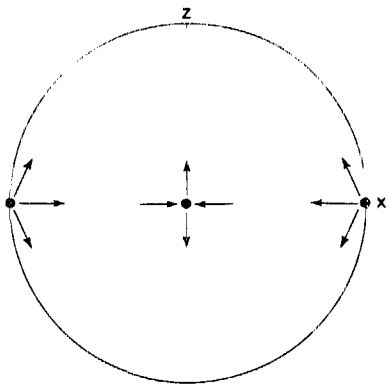

FIG. 20. The essential dynamical properties of phase shift schemes which generate pulse sequences for narrowband population inversion. Compare with Fig. 9. The instability of the equator of $SO(3)$ causes iterate sequences to produce complete inversion only at isolated values of the experimental parameters. The stability of the origin with respect to displacements in the xy plane produces no net rotation or a rotation about the z axis over large ranges of the experimental parameters.

$$T^{(\text{equator})} = \begin{pmatrix} 1.6708 & 0 \\ 0 & -0.0196 \end{pmatrix}. \tag{43}$$

The equator has one stable and one unstable direction. The unstable direction, with eigenvalue 1.6708, is the direction towards the origin. The stable direction, with eigenvalue -0.0196, is the z direction, as explained in Appendix A.

If the initial pulse sequence is a single π pulse, a displacement from the equator along z corresponds to a nonzero resonance offset. A displacement towards the origin corresponds to a nonzero difference $\omega_1 - \omega_1^0$. Loosely speaking, the equator of $SO(3)$ is stable with respect to the resonance offset and unstable with respect to the rf amplitude under [0,200,230,30,95]. Figure 26 shows inversion plots for the second iterate sequence generated by [0,200,230,30,95] for

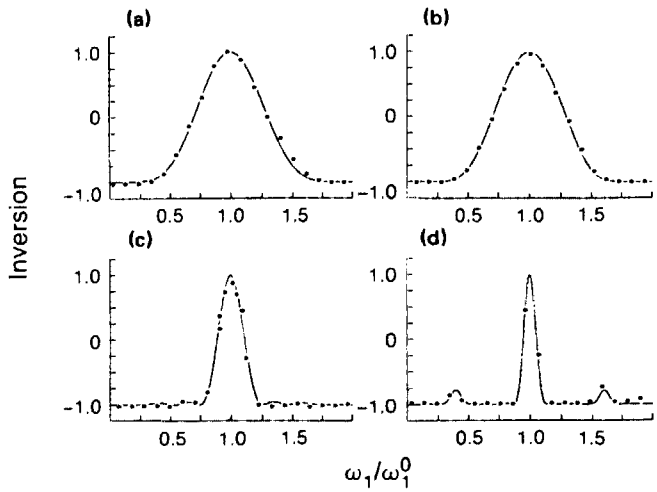

FIG. 21. Population inversion as a function of the rf amplitude for the first four iterates of a single π pulse, generated by [0,120,240] [(a)–(d), respectively]. Dots are experimental measurements, form ^{1}H NMR of a $H_2O_{(l)}$ sample. Lines are simulations. The function on $SO(3)$ that underlies [0,120,240] has the stability properties of Fig. 20.

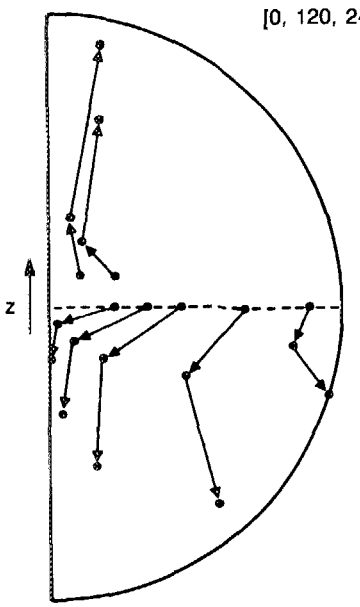

FIG. 22. The flow of points in $SO(3)$ under [0,120,240]. Points are rotated about z so as to lie in the xz plane. The escape of points from the xy plane results in the transient nature of the narrowband inversion profiles generated by [0,120,240] and seen in Fig. 21.

various, fixed offsets. As anticipated, the inversion is insensitive to the offset in a range of ω_1 about ω_1^0.

The results in Fig. 26 still suffer from a strong dependence on $\Delta\omega/\omega_1^0$ at values of ω_1 near $0.4\omega_1^0$ and $1.6\omega_1^0$. These ranges of ω_1 correspond to initial points in $SO(3)$ that are not near the equator and are therefore not controlled by the stability properties of the equator. It may be possible to generate pulse sequences for which the inversion is insensitive to $\Delta\omega/\omega_1^0$ over the entire range of ω_1 using iterative schemes with somewhat different stability properties. For example, if the entire xy plane of $SO(3)$ were stable with respect to displacements along z, and if the initial sequence was a single π pulse, then the resonance offset dependence could be canceled for all values of ω_1. Such stability properties cannot be achieved with iterative schemes that rely on phase shifts, but may be possible if other operations on pulse sequences are developed.

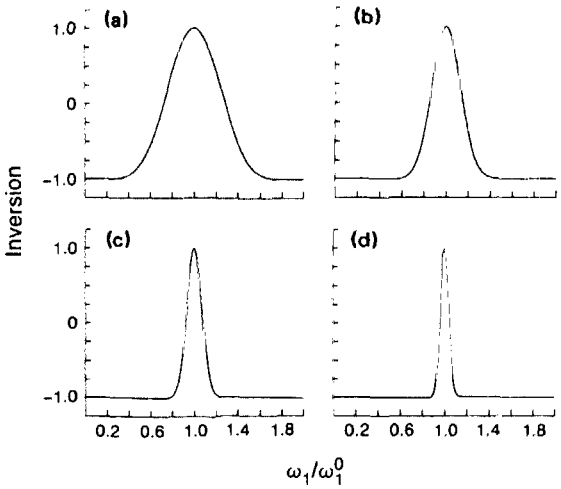

FIG. 23. Simulations of population inversion as a function of the rf amplitude for the first four iterates of a single π pulse generated by the scheme [104.5,255.5,0,255.5,104.5] [(a)–(d), respectively]. Compare with Fig. 21. [104.5,255.5,0,255.5,104.5] has the stability properties of Fig. 20, but the symmetry of the phase shifts prevents the escape of points from the xy plane in $SO(3)$, leading to a progressive, rather than transient, narrowing of the inversion profile.

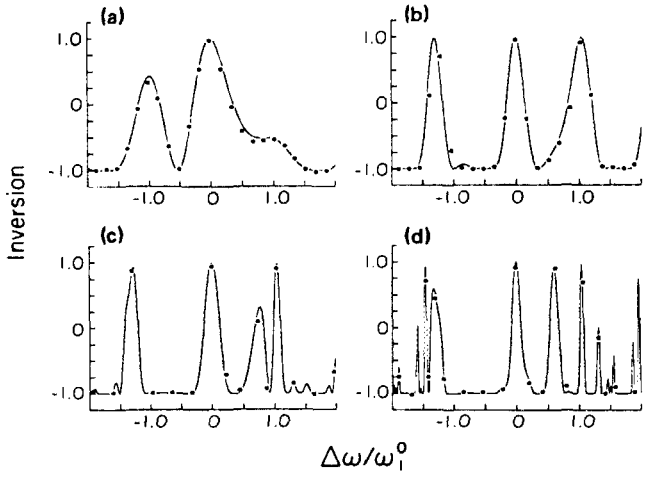

FIG. 24. Population inversion as a function of the resonance offset for the first four iterates of a single π pulse under [0,120,240]. Simulations (solid lines) and experimental data (dots) are shown. The development of multiple narrow offset ranges where populations are inverted is a common feature of iterative schemes that generate narrow inversion bandwidths with respect to the rf amplitude.

VI. FIXED POINT ANALYSIS OF OTHER ITERATIVE SCHEMES

A. Motivation

This section is devoted to analysis of iterative schemes developed by other authors for various purposes in NMR. We do not intend to give complete descriptions of either the theory or the applications of those schemes, but merely to demonstrate the applicability of the principles developed in the preceding sections to iterative schemes in general. Complete descriptions of the schemes, their derivations, and their applications can be found in the original papers. The fixed point theory yields geometrical pictures of those schemes and provides dynamical explanations of their performance.

B. Composite pulses

1. Recursive expansion procedure

Levitt and Ernst have proposed the recursive expansion procedure[5] for generating broadband composite $\pi/2$ pulses, i.e., pulse sequences which rotate the spin density operator from I_z to a linear combination of I_x and I_y. The recursive expansion procedure is an iterative scheme which may act on any initial pulse sequence in principle, but that depends on

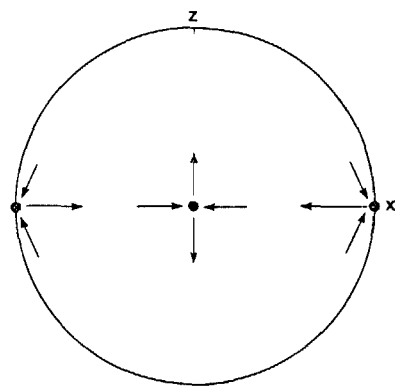

FIG. 25. Essential dynamic properties of phase shift schemes intended to generate narrowband inversion with respect to the rf amplitude over a broad range of resonance offsets. Compare with Fig. 14. The stability of the equator of $SO(3)$ with respect to displacements out of the xy plane is intended to remove the offset dependence of initial points near the equator.

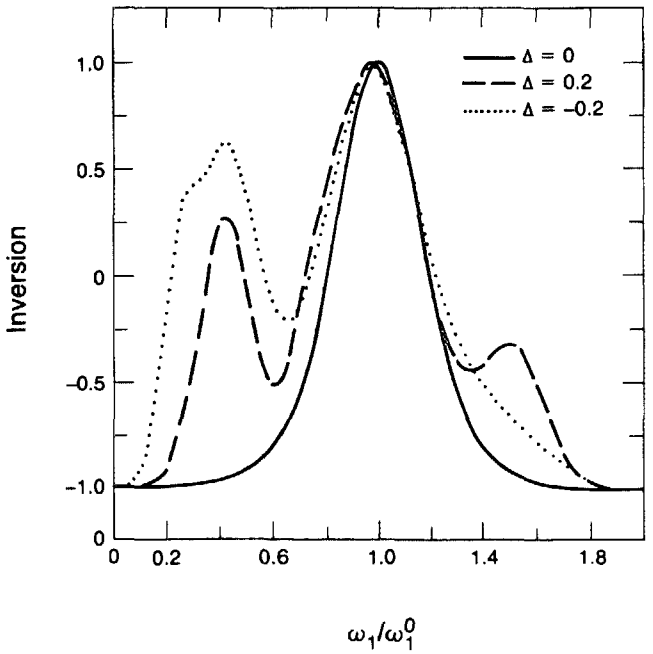

FIG. 26. Simulations of population inversion as a function of the rf amplitude for the second iterate of a single π pulse generated by [0,200,230,30,95]. This iterative scheme has the stability properties of Fig. 25. Plots for relative resonance offsets $\Delta = \Delta\omega/\omega_1^0$, values of 0.0, 0.2,and -0.2 are shown. The narrow inversion profile is fairly insensitive to the offset in a range of rf amplitudes ω_1 around the nominal value ω_1^0 around the nominal value ω_1^0, in contrast to the scheme [0,120,240] of Figs. 20–24.

the existence of an inverse sequence, i.e., another sequence that produces the inverse of the rotation produced by the initial sequence. When $\Delta\omega = 0$, an inverse sequence is easily constructed by phase shifting the initial sequence by 180° and reversing the order of the pulses. When $\Delta\omega \neq 0$, there is no general method for constructing an exact inverse, although Levitt and Ernst propose an approximate method.[5,65] In what follows, however, we assume that exact inverse sequences can always be found.

The recursive expansion procedure consists of concatenating the sequence S_0 with its inverse, phase shifted by 90°. Thus, the first iterate sequence S_1 can be symbolized by $S_0(S_0^{-1})_{90}$. A convenient general form for the initial rotation, or point in $SO(3)$, is

$$R(\alpha) = R_z(\gamma_1)R_x(\xi)R_z(\gamma_2). \tag{44}$$

Rotations that transform I_z to a linear combination of I_x and I_y have $\xi = \pi/2$ in Eq. (44). Note that such rotations do not necessarily produce a net rotation of $\pi/2$. They are merely the rotations that produce an inversion of zero.

The first iterate rotation $R(\beta)$ becomes

$$R(\beta) = R_z(\pi/2 - \gamma_2)R_x(\pi/2 + \epsilon) \times R_z(-\pi/2)R_x(\pi/2 + \epsilon)R_z(\gamma_2) \tag{45}$$

with

$$\xi = \pi/2 + \epsilon. \tag{46}$$

If Eq. (45) is evaluated to first order in ϵ, the result

$$R(\beta) = R_z(-\gamma_2 + \epsilon)R_x(\pi/2)R_z(\pi/2 + \gamma_2 + \epsilon) \tag{47}$$

is obtained. $R(\beta)$ is thus a rotation that transforms I_z to a linear combination of I_x and I_y. Such rotations are therefore a superstable, invariant set under the recursive expansion procedure. That set is a surface embedded in $SO(3)$, as shown in Fig. 27.

Figure 28 is a basin image for the recursive expansion procedure, illustrating the number of iterations required for convergence to the surface in Fig. 27. The recursive expansion procedure has rotational symmetry about the z axis, so that it is again sufficient to consider a single slice through $SO(3)$. The qualitative difference between Fig. 28 and Figs. 12 and 13 is striking. There is no fractal, nonconvergent set in Fig. 28. Rather, Fig. 28 reveals that the basin of the stable invariant set is the entire $SO(3)$ space, excluding the z axis and the equator. Initial points appear to converge in a smooth, structureless manner.

The simplicity of the dynamics for the recursive expansion scheme suggested by the simplicity of the basin image in Fig. 28 can be explained by representing the rotation operators as 3×3 matrices in the $\{x,y,z\}$ basis. We can then treat recursive expansion as a function acting on R_{zz}, the matrix element that specifies the extent of inversion. From Eq. (44), we have

$$[R(\alpha)]_{zz} = \cos\xi. \tag{48}$$

The first iterate $R(\beta)$ has the matrix element

$$[R(\beta)]_{zz} = \cos^2\xi. \tag{49}$$

Equations (48) and (49) show that the underlying one-dimensional mapping for the recursive expansion procedure is

$$f(x) = x^2. \tag{50}$$

f has a superstable fixed point at $x = 0$, with a basin that is the open interval $(-1,1)$, and an unstable fixed point at $x = 1$.

With $x = \cos\xi$, the superstable fixed point is at $\xi = \pi/2$, corresponding to the surface in Fig. 27, and the basin is the open interval $(0,\pi)$, corresponding to the entire $SO(3)$ space excluding the z axis and the equator. The lines that separate differently shaded regions in Fig. 28 are cross sections through surfaces of constant ξ embedded in $SO(3)$.

2. Retrograde compensation

Shaka and Freeman[6] have proposed iterative schemes which generate pulse sequences for narrowband inversion,

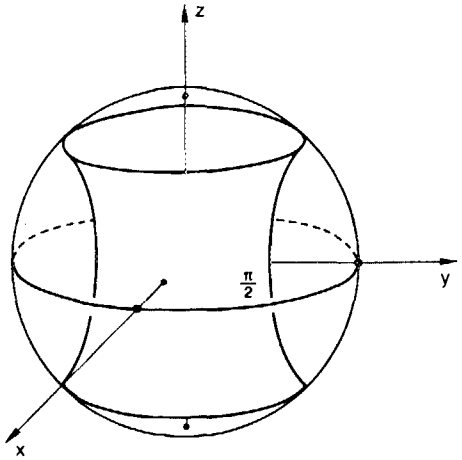

FIG. 27. The surface in $SO(3)$ comprising the locus of points that correspond to rotations creating transverse (xy) magnetization when acting on a density operator I_z, i.e., "generalized $\pi/2$ rotations."

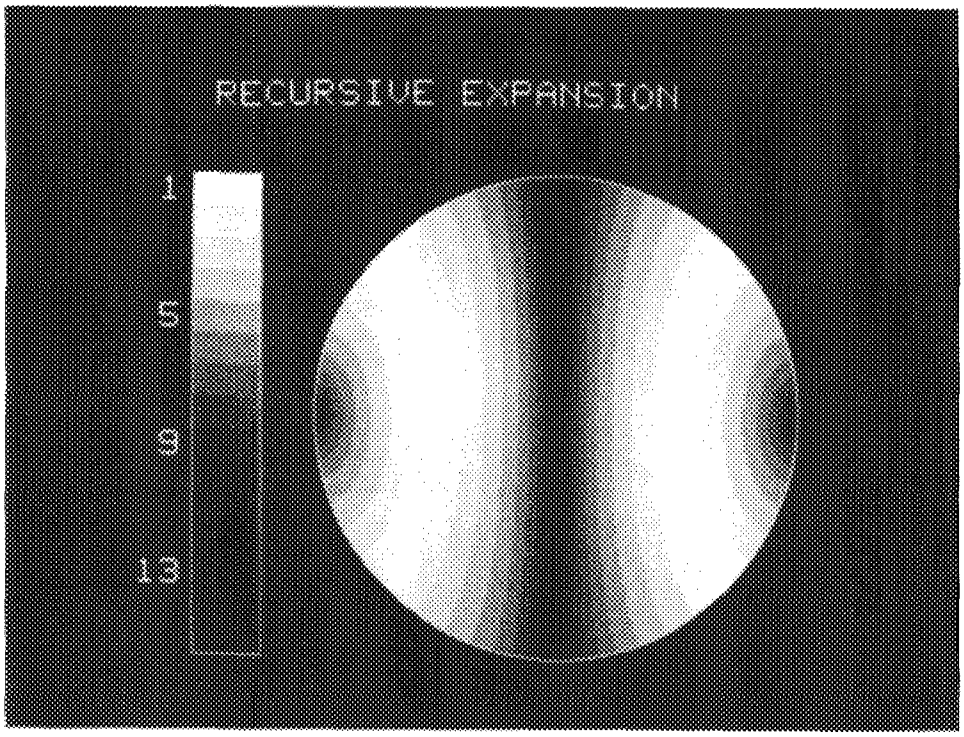

FIG. 28. Basin image for the recursive expansion scheme of Levitt and Ernst designed to produce $\pi/2$ rotations which are broadband in ω_1. The basin of the surface in Fig. 27 is shown in a cross section of $SO(3)$ containing the z axis. The basin is the entire space, excluding the z axis and the equator.

which they refer to as retrograde compensation. As with the recursive expansion procedure discussed above, the retrograde schemes use inversion, phase shifting, and concatenation operations. One scheme is defined by $S = S_0(S_0^{-1})_{60}(S_0)_{120}$, i.e., a concatenation of the initial sequence, the inverse sequence phase shifted by 60°, and the initial sequence phase shifted by 120°. For this scheme, the equator of $SO(3)$ is an unstable invariant set. However, every point on the z axis is superstable with respect to displacements in the xy plane. To see this, write the initial point $R(\alpha)$ in the general form

$$R(\alpha) = R_z(\gamma)R(\epsilon), \tag{51}$$

where the z component of ϵ is zero. The first iterate $R(\beta)$ is then

$$R(\beta) = R_z(\gamma + 2\pi/3)R(\epsilon)R_z(-\pi/3)R(-\epsilon) \times R_z(-\pi/3)R(\epsilon). \tag{52}$$

If $|\epsilon|$ is small, $R(\alpha)$ is close to the z axis of $SO(3)$. To first order in $|\epsilon|$, Eq. (52) reduces to

$$R(\beta) = R_z(\gamma), \tag{53}$$

demonstrating that each point on the z axis is individually fixed and superstable.

Figure 29 is a basin image for the retrograde scheme. As with the recursive expansion procedure discussed earlier, the basin image suggests simple dynamics. All initial points not on the equator apparently converge smoothly to the z axis. Again, it can be shown that there is an underlying one-dimensional mapping whose properties imply the simplicity of Fig. 29. If the initial point in $SO(3)$ is written in the form of Eq. (44), then Eq. (48) still holds. Equation (49) is replaced by

$$[R(\beta)]_{zz} = \tfrac{1}{4}\cos^3\xi - \tfrac{3}{4}\cos^2\xi + \tfrac{3}{4}\cos\xi + \tfrac{3}{4}. \tag{54}$$

The underlying mapping is, therefore

$$g(x) = \tfrac{1}{4}(x^3 - 3x^2 + 3x + 3). \tag{55}$$

g has a superstable fixed point at $x = 1$ and an unstable fixed point at $x = -1$ corresponding to the superstable and unstable fixed points at the z axis and the equator, respectively. In addition, g has an unstable fixed point at $x = 3$ which has no analog in the function on $SO(3)$. All initial values of x in the interval $(-1,1)$ converge to 1 under iterations of g. Therefore, all initial points in $SO(3)$ for which ξ is in the interval $(0,\pi)$, which is to say the entire space excluding the equator and the z axis, converge to the z axis.

Pulse sequences generated by applying the $S_1 = S_0(S_0^{-1})_{60}(S_0)_{120}$ scheme to an initial single π pulse exhibit population inversion performance as a function of the rf amplitude very similar to the results in Fig. 23. Shaka and Freeman also propose a scheme represented by $S = S_0(S_0^{-1})_{90}(S_0)_{180}$ for generating narrowband inversion sequences. The latter scheme has the property that, when viewed as a function on SO(3), it maps the surface in Fig. 27 onto the z axis. This property results in the narrowband inversion features of the iterate sequences. However, linearization near the z axis leads to eigenvalues of $\pm i$, so that initial points near the z axis do not converge geometrically to the z axis.

C. Heteronuclear decoupling sequences for liquid state NMR

1. Waugh sequences

Beginning with the MLEV schemes of Levitt and Freeman,[33] several authors have demonstrated pulse sequences[3,4,33–38] and iterative schemes for generating such sequences,[3,4] designed to remove heteronuclear couplings in liquid state NMR, e.g., to decouple protons from ^{13}C nuclei, allowing the observation of the ^{13}C spectrum without line splittings caused by the coupled protons. The decoupling sequences are designed to be effective over a large range of proton resonant frequencies. Waugh has given a criterion for

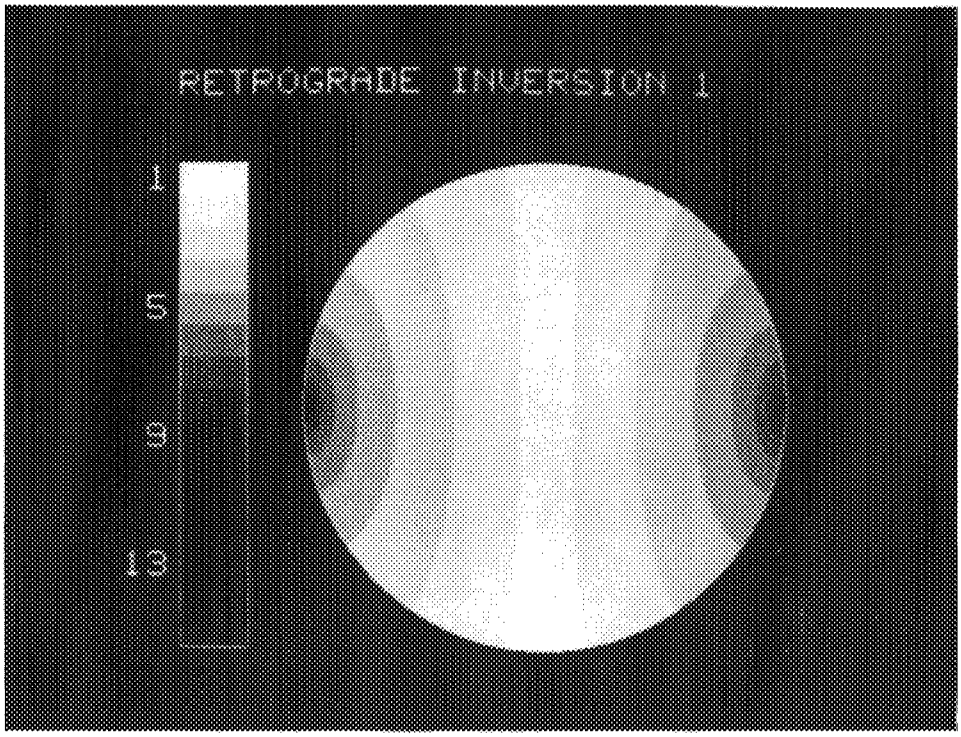

FIG. 29. Basin image for the retrograde compensation scheme of Shaka and Freeman. This scheme generates narrowband inversion sequences. The basin of the z axis is shown, in a cross section of $SO(3)$ containing the z axis. The basin is the entire space, excluding the equator. The equator is an unstable invariant set.

evaluating liquid state decoupling sequences[36]: a good decoupling sequence is one for which the net rotation experienced by an isolated spin is independent of the resonance offset over a large range of offsets. In addition, Levitt, Freeman, and Frenkiel[3] and Waugh[4] have demonstrated particular iterative schemes yielding pulse sequences which produce net rotations of nearly zero over a large range of offsets. These constitute efficient decoupling sequences.

Waugh's criterion reduces the decoupling problem to the consideration of the response of an isolated spin to the pulse sequence. The relevant propagator space is therefore $SO(3)$. However, because both the MLEV scheme of Levitt, Freeman, and Frenkiel and the Waugh scheme involve the permutation of pulses, they do not yield unique functions on $SO(3)$. This can be seen in general from the following argument. Suppose the initial sequence, with propagator U, is composed of M pulses with propagators V_i. Then;

$$U = V_M V_{M-1} \cdots V_1. \tag{56}$$

Permuting a pulse gives a new version of the sequence with a propagator U_p:

$$U_p = V_{M-1} \cdots V_1 V_M \tag{57}$$

$$= V_M^{-1} U V_M. \tag{58}$$

Since the transformation V_M depends on parameters in the Hamiltonian, for example, ω_1 and $\Delta\omega$, as well as the phase of the permuted pulse, the relationship between U and U_p depends on those parameters. If the scheme involves permuting pulses, the initial point in the propagator space does not alone determine the series of iterate points. That series depends on the Hamiltonian parameters and the precise form of the initial sequence.

Waugh's scheme may be applied to any initial sequence of $\pi/2$ pulses. One version of the scheme is to permute a $\pi/2$ pulse from the end of the sequence to the beginning, to form a version of the permuted sequence with an overall phase shift of 180°, and finally to concatenate the permuted sequence with the phase-shifted, permuted sequence. The scheme generates a new sequence that is also composed of $\pi/2$ pulses, so that the scheme may be applied iteratively.

Despite the fact that there is no unique function on $SO(3)$, we can apply a fixed point analysis to Waugh's scheme with some modification. First, we show that the origin of $SO(3)$ is a stable fixed point, as shown in Fig. 30, over particular ranges of ω_1 and $\Delta\omega$. Suppose that the initial rotation is $R(\alpha)$. If the phase of the last $\pi/2$ pulse in the initial pulse sequence is 0, then the net rotation of the first iterate sequence is $R(\beta)$:

$$R(\beta) = R_z(\pi)R(\chi)R(\alpha)R(-\chi)R_z(-\pi)R(\chi)R(\alpha)R(-\chi). \tag{59}$$

$R(\chi)$ is the rotation produced by the permuted $\pi/2$ pulse, as a function of ω_1 and $\Delta\omega$:

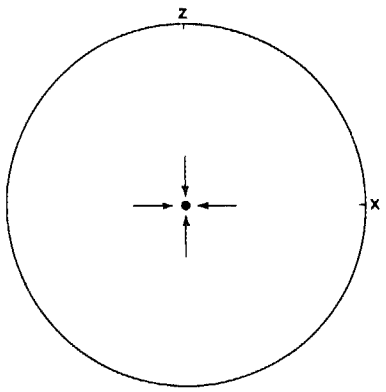

FIG. 30. Implementation of heteronuclear decoupling by making the origin of $SO(3)$ superstable in all directions. This generates the unit operator with increasing iterations.

$$\chi = \pi(\omega_1,0,\Delta\omega)/(2\omega_1^0). \tag{60}$$

If $R(\alpha)$ is the unit operator, then so is $R(\beta)$, which implies that the origin of $SO(3)$ is a fixed point. If Eq. (59) is evaluated to first order in $|\alpha|$, the result

$$\beta = [0,0,2\alpha_x \cos\theta \sin\theta(1-\cos\chi) + 2\alpha_y \sin\chi\cos\theta + 2\alpha_z(\cos^2\theta\cos\chi + \sin^2\theta)] \tag{61}$$

is obtained, with

$$x = |\chi|, \tag{62}$$

$$\tan\theta = \Delta\omega/\omega_1. \tag{63}$$

The linear transformation relating β and α in Eq. (61) has a doubly degenerate eigenvalue of 0. The third eigenvalue is λ_W, given by

$$\lambda_W = 2(\cos^2\theta\cos\chi + \sin^2\theta). \tag{64}$$

The eigenvector with eigenvalue λ_W is (0,0,1). This eigenvector and eigenvalue are independent of the phase of the permuted pulse. In addition, the same eigenvalues and the eigenvector (0,0,1) are obtained if a $\pi/2$ pulse is permuted from the beginning of the initial sequence to the end, rather than from the end to the beginning, or if the order of concatenation is reversed.

In the language of the fixed point theory, it is the stability of the orgin of the propagator space $SO(3)$, namely the behavior in Fig. 30, that causes the Waugh scheme to generate pulse sequences producing net rotations of nearly zero over a range of resonance offsets and rf amplitudes. Equation (64) specifies precise limits on those parameters for which the origin is in fact stable, i.e., for which $\lambda_W \leqslant 1$. The limits specified by Eq. (64) therefore suggest the maximum decoupling bandwidths attainable with the Waugh scheme. For example, if $\omega_1 = \omega_1^0$, the origin is stable if $|\Delta\omega| \leqslant 1.732\omega_1^0$. If $\Delta\omega = 0$, the origin is stable if $2\omega_1^0/3 \leqslant \omega_1 \leqslant 4\omega_1^0/3$.

The decoupling bandwidths achieved by specific iterate pulse sequences depend not only on the stability of the origin, but also on the choice of the initial sequence and on the dynamics of the iterative scheme over the entire $SO(3)$ space. In Sec. IV, basin images were used to reveal the dynamics of iterative schemes for broadband population inversion and to guide the choice of initial sequences. The absence of a unique function on $SO(3)$ makes the treatment of decoupling schemes less straightforward. For the Waugh scheme, it is still possible to construct a basin image, if we take the following conditions:

1. Only a single combination of $\Delta\omega$ and ω_1 values is considered at a time.

2. Both the direction of permutation and the order of concatenation are reversed from one iteration to the next, in such a way that the same $\pi/2$ pulse is permuted each time.

3. The permuted pulse is assumed to have a phase of 0. Basin images for various offsets, with $\omega_1 = \omega_1^0$, are shown in Fig. 31. For the Waugh scheme, there is no rotational symmetry about the z axis, so that it is necessary to specify the azimuthal angle of the pictured slice. The images in Fig. 31 hold for initial points in the xz plane. If, as in Ref. 49, the initial pulse sequence is four $\pi/2$ pulses of phase 0, i.e., a single 2π pulse, then initial points for all values of ω_1 and $\Delta\omega$ do in fact lie in the xz plane.

Figure 31 indicates that the size of the region of the xz plane of $SO(3)$ that converges rapidly to the origin decreases as the offset increases and the origin makes the transition from superstability to instability. The dynamics become apparently more complex. Note that at $\Delta\omega = 2\omega_1^0$, where $\lambda_W = 1.227$, there are still certain initial points that do converge to the origin. The origin still has two superstable directions. The overall instability of the origin is reflected in the fact that not all initial points near the origin coverge to the origin.

Basin images such as those in Fig. 30 can be used to guide the selection of an initial pulse sequence, although the procedure is necessarily somewhat different from that employed in Sec. IV. One approach would be to define an offset-independent basin for the iterative scheme as the intersection of the basins for all offsets in the relevant range. A search for an initial sequence whose locus of points in $SO(3)$ lies within the offset-independent basin could then be conducted. A second, less restrictive approach would be to search for an initial sequence such that, for each particular offset value, the single point in $SO(3)$ lies within the rapidly convergent region for that offset.

It has been demonstrated, although without a fixed point analysis, that the decoupling bandwidth of pulse sequences generated by the Waugh scheme can be enlarged by the use of an appropriate initial sequence.[37,38]

2. MLEV sequences

Levitt, Freeman, and Frenkiel have developed an iterative scheme that generates pulse sequences for heteronuclear decoupling known as MLEV-4, MLEV-16, etc.[3] The development of the MLEV sequences has stimultated much of the subsequent work on decoupling and composite pulses. With Waugh's criterion for evaluating decoupling sequences in mind, we can analyze the MLEV scheme in terms of its fixed point properties in $SO(3)$.

The MLEV scheme operates on an initial sequence composed of an even number of composite π pulses. The composite π pulses are all of the same type, with overall phases of either 0° or 180°. Four versions of the initial sequence are formed: the initial sequence itself, the initial sequence with an overall phase shift of 180°, the initial sequence with one composite π pulse permuted from the end to the beginning, and the permuted sequence with an overall phase shift of 180°. In the simplest case of the MLEV scheme, the four versions are concatenated to form an iterate sequence. Although the full MLEV theory allows considerably more flexibility in the construction of iterates, we consider only the simplest case as an example.

Assume that the initial sequence produces a net rotation $R(\alpha)$, and that the permuted composite pulse produces a rotation P. Then the rotation produced by the first iterate sequence is $R(\beta)$:

$$R(\beta) = R_z(\pi)PR(\alpha)P^{-1}R_z(-\pi)P \times R(\alpha)P^{-1}R_z(\pi)R(\alpha)R_z(-\pi)R(\alpha). \tag{65}$$

If $R(\alpha)$ is the unit operator, then so is $R(\beta)$. The origin of $SO(3)$ is therefore fixed. If we express P in the general form

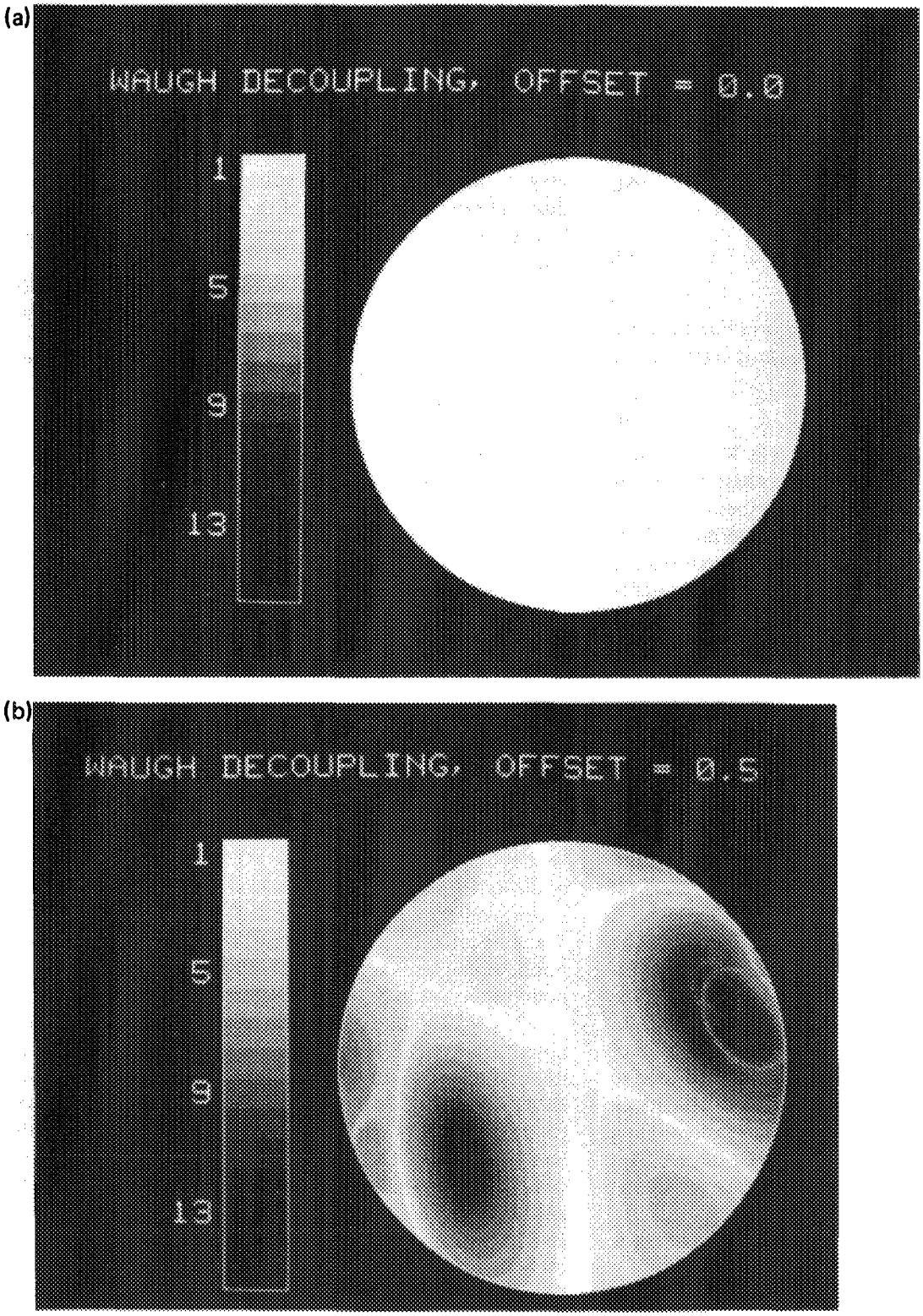

FIG. 31. Basin images corresponding to the iterative scheme for heteronuclear decoupling developed by Waugh. In this case, the underlying function on $SO(3)$ depends on the resonance offset. Basins of the origin of $SO(3)$ are shown for resonance offsets $\Delta\omega/\omega_1^0$ equal to 0.0 (a), 0.50 (b), 1.0 (c), and 2.0 (d), in the xz plane of $SO(3)$. The basin decreases in size with increasing offset. In (d), the origin is unstable.

$$P = R_z(\eta_1)R_x(\eta_2)R_z(\eta_3), \tag{66}$$

we can evaluate Eq. (65) to first order in $|\alpha|$:

$$\beta = [0,0,2\sin\eta_2\sin\eta_3\alpha_x + 2\sin\eta_2\cos\eta_3\alpha_y + 2(\cos\eta_2 + 1)\alpha_z]. \tag{67}$$

Equation (67) bears an obvious resemblance to Eq. (61), so that the dynamics of the MLEV and Waugh schemes are similar in the neighborhood of the origin. The linear transformation relating α and β in Eq. (67) has a doubly degenerate eigenvalue of 0 and a third eigenvalue λ_M given by

$$\lambda_M = 2(\cos\eta_2 + 1). \tag{68}$$

In view of Eq. (66), the extent of population inversion pro-

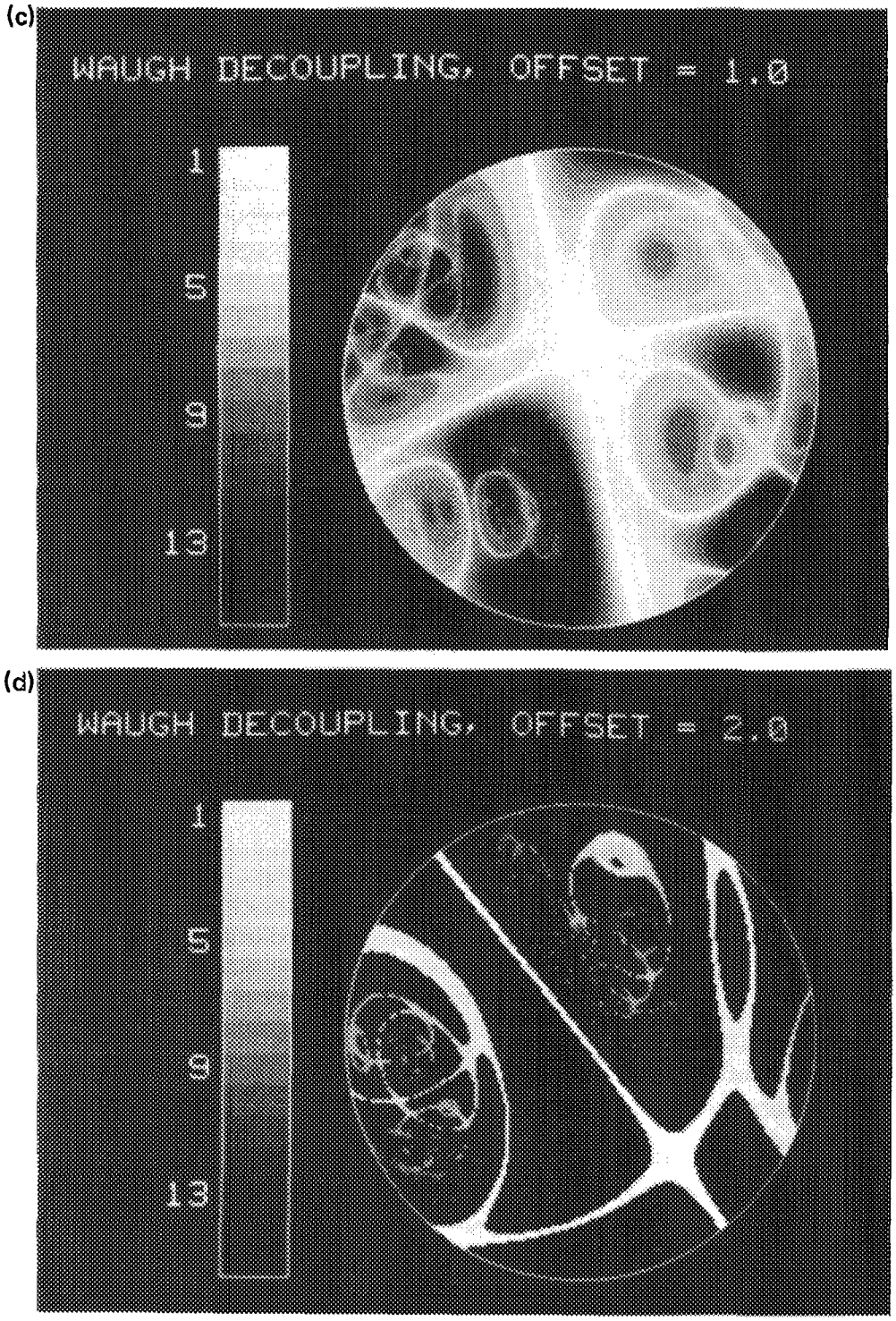

FIG. 31. (*continued*)

duced by the composite π pulses that comprise the MLEV sequences is $-\cos\eta_2$. Equation (68) then implies that the stability condition $\lambda_M < 1$ is the same as the condition that the composite π pulses produce an inversion greater than 1/2. For a given form of composite π pulse, this inversion requirement dictates particular ranges of ω_1 and $\Delta\omega$.

D. Selective excitation of multiple quantum coherence

Iterative schemes have been developed for selectively exciting multiple quantum coherences in coupled spin systems.[2] The objective is to excite coherences only between spin states that differ in their Zeeman quantum number by a multiple of a particular integer n, i.e., nk-quantum coherences. In a coupled spin system, the effect of a pulse sequence is not necessarily to produce a rotation. Rather, the propagator for the initial sequence is a general unitary transformation U_0, which may be written in terms of irreducible tensor operators $T_{lm}(q)$[66]:

$$U_0 \exp(-iA), \tag{69}$$

$$A = \sum_q \sum_l \sum_{m=-l}^{l} C_{lm}(q)\, T_{lm}^{(q)}. \tag{70}$$

The index q is necessary because there may be several independent operators with the same l and m. A must be Hermitian, which implies

$$C_{l-m}(q) = (-1)^m C_{lm}(q)^*. \tag{71}$$

For any particular arrangement of coupled spins, the propagator space is a subspace of the space of operators in the form of Eqs. (69) through (71). The real and imaginary parts of the coefficients $C_{lm}(q)$ may be treated as the coordinates of points in the multidimensional propagator space, just as the components of α are the coordinates of the point $R(\alpha)$ in $SO(3)$.

The selective excitation scheme employs the phase shifting and concatenation operations discussed in Sec. III, but without the restriction to odd N. The scheme $[0,1\times360/n,2\times360/n,\ldots,(n-1)\times360/n]$ is used for selective nk-quantum excitation. Since an overall rf phase shift of ϕ has the effect of rotating the propagator about z by ϕ, the propagator for the first iterate sequence is U_1, given by

$$U_1 = U_0^{(n-1)}\, U_0^{(n-2)} \cdots U_0^{(1)}\, U_0^{(0)} \tag{72}$$

with

$$U_0^{(P)} = \exp(-iA^{(P)}), \tag{73}$$

$$A^{(p)} = \sum_q \sum_l \sum_{m=-l}^{l} \exp[-im(2\pi p/n)]\, C_{lm}(q) T_{lm}(q). \tag{74}$$

Equation (74) depends on the property of irreducible tensor operators that

$$R_z(\phi)\, T_{lm}(q) R_z(-\phi) = \exp(-im\phi)\, T_{lm}(q). \tag{75}$$

Since U_1 is uniquely determined by U_0, the scheme defines a function on the propagator space. The function has a fixed point at the origin, because U_1 is the unit operator if U_0 is the unit operator. To evaluate the stability of the origin, we can evaluate U_1 to first order in the magnitudes of the coefficients $C_{lm}(q)$ by adding the exponents $A^{(p)}$. Using the identity

$$\sum_{p=0}^{n-1} \exp[-im(2\pi p/n)] = \begin{cases} n, & m \text{ a multiple of } n \\ 0, & \text{otherwise} \end{cases}, \tag{76}$$

we find

$$U_1 = \exp(-iA_T), \tag{77}$$

$$A_T = n \sum_q \sum_l \sum_m{}' C_{lm}(q) T_{lm}(q), \tag{78}$$

where the sum over m in Eq. (78) is restricted to multiples of n. Since U_1 in Eq. (77) contains only irreducible tensor operators with m a multiple of n, it transforms a spin system from equilibrium to a state with only nk-quantum coherences.

Equation (78) reveals that the origin is unstable, with eigenvalue n, with respect to displacements along axes in the propagator space that correspond to $T_{lm}(q)$ operators with m a multiple of n. The origin is superstable along other axes. Initial points near the origin move towards the origin along the superstable directions and away from the origin along the unstable directions upon iteration, as shown in Fig. 32. Since the $T_{lm}(q)$ axes with m a multiple of n are not themselves stable, however, the generation of nk-quantum selective propagators is a transient result of the iterative scheme. Once a point is far enough from the origin that the linearization leading to Eq. (77) is not valid, small contributions of undesired tensors may become larger, thus destroying the selectivity. The situation is analogous to the transient generation of narrowband inversion sequences by the scheme [0,120,240], as discussed in Sec. V.

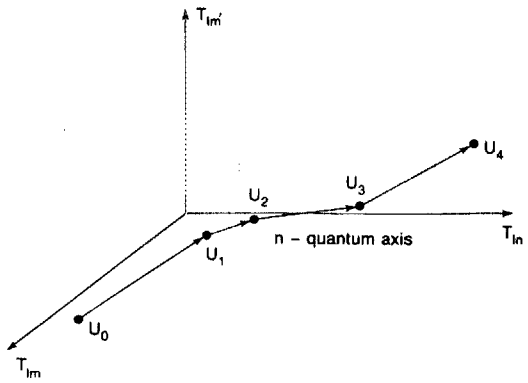

FIG. 32. Dynamics of the iterative schemes for selective excitation of n-quantum coherence. The propagator space is a multidimensional space in which the axes may be labeled as components of irreducible tensor operators T_{lm}. For a phase-shifting scheme with phase $\phi = 2\pi/n$, the origin is superstable with respect to displacements along all axes except for those for which m is a multiple of n. A propagator that lies on such an axis only excites coherences whose orders are a multiple of n. A hypothetical flow of points in the propagator space is shown. Note that points may escape from the n-quantum axis when they are far from the origin. A more efficient n-quantum excitation scheme would involve making the T_{ln} axis stable.

The selective excitation schemes of Warren *et al.*[2] were originally derived using average Hamiltonian theory. Theorems concerning the average Hamiltonian of a pulse sequence that is the concatenation of shorter sequence units, as developed by Burum *et al.*[30] and Warren *et al.*[2] were employed. Due to its nature as a power series expansion, the application of average Hamiltonian theory to the very long sequences generated by an iterative scheme raises questions of convergence. Warren *et al.* dealt with the convergence problem by using a "time reversal sandwich" sequence as the initial pulse sequence. The time reversal sandwich has a propagator that lies close to the origin in the propagator space but at the same time has significant components of high-order multiple quantum tensors. The fixed point analysis above also indicates that the selective excitation scheme will only act effectively on an initial propagator near the origin, although that conclusion is reached from a consideration of fixed points and their stability rather than a consideration of questions of the convergence of a series expansion.

The MLEV decoupling sequences described above were also originally analyzed in terms of average Hamiltonian theory.[3] As a complement to average Hamiltonian theory, the fixed point theory provides a unified description of the properties of iterative schemes. A fixed point analysis also furnishes the context for an investigation of the global dynamics of an iterative scheme, i.e., the dynamics over the entire propagator space. The fact that particular iterative schemes can be treated both by average Hamiltonian theory and by the fixed point theory suggests that there exists a connection between the two theoretical approaches, despite

their differences in viewpoint. One aspect of that connection is the similarity between the calculation of a zeroth order average Hamiltonian and the assessment of the stability of a fixed point, both of which are linearization processes. In Appendix C, we outline a subtle connection between the two theories which extends to all orders of the average Hamiltonian and all orders of iteration.

VII. CONCLUSION

A. Benefits of the fixed point theory

The previous sections serve to demonstrate the wide applicability of the fixed point theory as a mathematical background for the analysis and development of iterative schemes for generating excitation sequences. While iterative schemes have been developed by other authors without using the methods presented in this paper, the fixed point theory is an advance over previous approaches in several important areas. First, a unified set of concepts and the accompanying geometrical picture allow visualizations and comparisons of schemes and explanations of their essential features to be made. These concepts include the propagator space, functions on the propagator space, fixed points of the functions, stability of the fixed points, basins of stable fixed points, and loci of initial points. Second, the fixed point theory demonstrates the importance of considering the action of an iterative scheme on the entire range of possible initial pulse sequence propagators, i.e., the dynamics on the entire propagator space. Features of a scheme such as the presence or absence of fractal, nonconvergent sets, the sizes and shapes of basins, symmetry restrictions, and the existence of unanticipated fixed points may have dramatic effects on the excitation properties of the sequences that are generated. A knowledge of these features allows comparisons of proposed schemes to be made and aids in the optimization of the performance of a scheme by suitable choice of an initial sequence. Global features of the dynamics of an iterative scheme are often clearly revealed by numerical procedures such as the generation of basin images. Third, dynamical concepts allow a clear treatment of schemes that otherwise would not be considered or could only be treated with difficulty. For example, traditional average Hamiltonian theory calculations are concerned with making an error term in the propagator vanish entirely. In the language of dynamics, this is the case of superstability. However, as shown in this paper, useful results are obtained from schemes in which fixed points are stable, but not superstable. Fixed points that are unstable, or stable in some directions and unstable in others, also lead to interesting and useful results.

B. Further applications

To conclude, we briefly discuss several extensions and generalizations of the work described in the previous sections.

The treatment of phase shift schemes in Sec. III–V concentrates on their applications to population inversion, either broadband or narrowband, in systems of isolated spins. Thus, the emphasis is on generating net rotations of π. Similarly, phase shift schemes that generate broadband or narrowband $\pi/2$ rotations may be constructed. Possible stability properties for such schemes are shown in Fig. 33. As an example, the scheme [0,135,135,0] generates $\pi/2$ rotations that are broadband with respect to the rf amplitude when applied to an initial single $\pi/2$ pulse. This result is shown in Fig. 34. An analogous narrowband $\pi/2$ sequence would potentially be quite useful in spatial localization experiments that rely on rf field gradients.[6,20–22] Note that, in contrast to the recursive expansion procedure[5] discussed in Sec. VI B, [0,135,135,0] generates pulse sequences that produce net rotations of strictly $\pi/2$ radians. This is because the stable invariant set is the circle in Fig. 33(a), rather than the surface in Fig. 27.

A more complex problem than simply minimizing or maximizing the excitation bandwidth of pulse sequences is the problem of tailoring the bandwidth, i.e., producing nearly complete excitation within specified ranges of some experimental parameter and no excitation outside of these ranges. A possible approach to this problem is the construction of an iterative scheme with more than one fixed point.[67] Consider, for example, the case of two stable fixed points, one at the origin of the propagator space and the other at a point that represents the desired excitation. As shown in Fig. 35, each fixed point may have its own basin, with the two basins separated by a boundary. If the initial pulse sequence is chosen so that initial points in the propagator space lie in the basin of one fixed point over the specified range of the parameter and in the basin of the other fixed point for other values of the parameter, then the desired excitation profile may be achieved in the iterate sequences. An example of this is the development of an ω_1-selective π pulse with a sharp rectangular bandwidth.[67]

Lastly, the development of iterative schemes for excitation in coupled spin systems, or multilevel spectroscopic systems in general, is an area that remains largely unexplored. Obvious goals include the design of schemes for population inversion and the excitation of transverse magnetization over large ranges of spin coupling constants. Improved schemes for the selective excitation of multiple quantum coherences are also desirable. As suggested by Fig. 32, a scheme under which the entire n-quantum axis is a stable invariant set would overcome the transient nature of the existing schemes. Schemes for heteronuclear and homonuclear

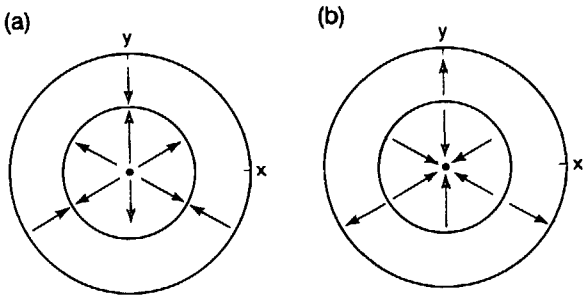

FIG. 33. Dynamical properties of iterative schemes for generating broadband (a) and narrowband (b) $\pi/2$ rotations. Shown is the xy plane of $SO(3)$. The origin is a fixed point. The circle at a radius of $\pi/2$ from the origin is an invariant set. For broadband excitation, the origin is unstable and the circle is stable. For narrowband excitation, the origin is stable and the circle is unstable.

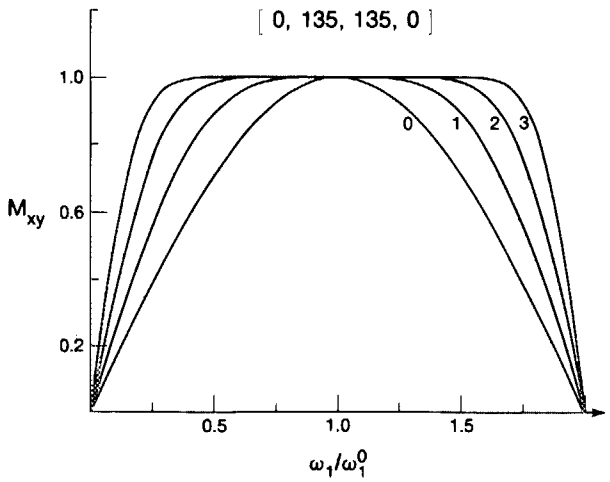

FIG. 34. Simulations of the transverse magnetization M_{xy} excited as a function of the rf amplitude for pulse sequences generated by the scheme [0,135,135,0] which has the stability properties of Fig. 32(a). Shown are results from a single $\pi/2$ pulse and its first three iterates, labeled 0–3, respectively.

decoupling in systems of many coupled spins may lead to improvements over the decoupling sequences that are currently in use. Stabilizing the origin of a multidimensional propagator space with respect to all directions is tantamount to complete decoupling, homonuclear or heteronuclear. A similarity between the selective excitation and decoupling problems exists, *since a pulse sequence that is strictly* $\geqslant(n+1)$*-quantum selective will decouple a system of n spins.* n spins cannot absorb or emit more than n quanta.

The application of the fixed point theory to the problems mentioned above will require further developments in several areas. The algebraic procedures that lead to the discovery of fixed points and the determination of their stability will require a careful study of the properties of irreducible tensor operators. Efficient numerical methods for treating functions on a multidimensional propagator space must be developed. In fact, even the structure of the propagator space for a coupled spin system, analagous to $SO(3)$ for an isolated spin, is not immediately apparent.

Finally, a crucial component of the development of new iterative schemes is likely to be the discovery of new approaches that can be performed on an initial pulse sequence, specifically operations that affect the pulse sequence propagator in some well-characterized way. In summary, there remains ample place for experience, intuition, and inspiration in the design of excitation sequences for coherent spectroscopy.

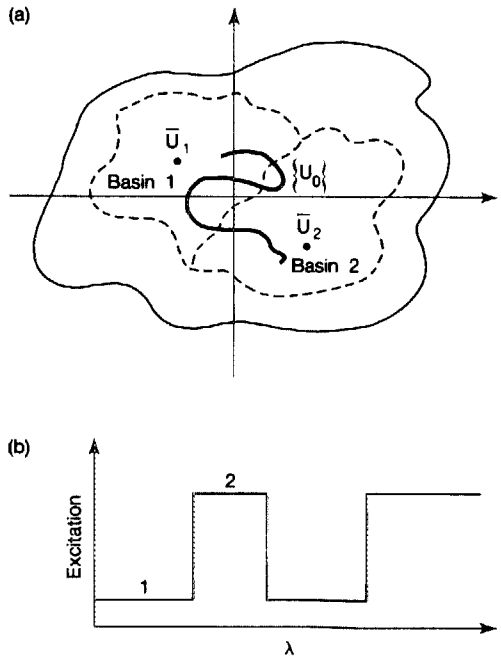

FIG. 35. A fixed point theory approach to tailored excitation. In (a), a propagator space with two stable fixed points is shown. Around each fixed point is its basin, indicated by the dashed lines. An initial pulse sequence is chosen so that the corresponding locus of points in the propagator space $\{U_0\}$ resulting from variatons in the experimental parameter λ, indicated by the solid line, crosses the boundary between the basins at specified values of λ. In (b), the anticipated excitation profile of iterate sequences is shown. The excitation takes on primarily two values as a function of λ, i.e., the values that correspond to the propagator $\bar{U}_1$ and the propagator $\bar{U}_2$. Thus the iterative scheme can generate a bistable response, allowing shaping of specific excitations and bandwidths.

ACKNOWLEDGMENTS

We thank J. Baum and H. Cho for assistance with the calculations and graphics and M. Mehring for critically commenting on the manuscript. R. T. was a National Science Foundation graduate fellow. A. P. was an Alexander von Humbolt Fellow at the Institute of Solid State Physics, University of Stuttgart. We are grateful to I. Procaccia and J. Jeener for some helpful discussions. J. G. was supported by the National Science Foundation and by the Air Force Office of Scientific Research. This work was supported by the Director, Office of Energy Research, Office of Basic Energy Sciences, Materials Sciences Division of the US Department of Energy and by the Director's Program Development Funds of the Lawrence Berkeley Laboratory under Contract No. DE-AC03-76SF00098.

APPENDIX A: EXPRESSION OF ROTATIONS NEAR THE EQUATOR OF *SO(3)*

In Eq. (23), the arbitrary rotation $R(\alpha)$ is expressed as the product of two rotations about axes in the xy plane:

$$R(\alpha) = R_\gamma(\pi)R(\epsilon). \tag{A1}$$

In this Appendix, we prove the generality of this expression by showing that γ can always be chosen such that the z component of ϵ is zero. This is equivalent to the requirement that

$$R_z(\pi)R(\epsilon)R_z(-\pi) = R(-\epsilon) \tag{A2}$$

or

$$R_z(\pi)R(\epsilon)R_z(-\pi)R(\epsilon) = 1. \tag{A3}$$

Using Eq. (A1), we have

$$R_z(\pi)R(\epsilon)R_z(-\pi)R_z(\epsilon)$$

$$= R_z(\pi)R_\gamma(-\pi)R(\alpha)R_z(-\pi)R_\gamma(-\pi)R(\alpha) \tag{A4}$$

$$= R_{\gamma+\pi/2}(-\pi)R(\alpha)R_{\gamma+\pi/2}(\pi)R(\alpha). \tag{A5}$$

In going from Eq. (A4) to Eq. (A5), we use the identities

$$R_z(\pi)R_y(-\pi) = R_{\gamma+\pi/2}(-\pi), \tag{A6}$$

$$R_{\gamma-\pi/2}(-\pi) = R_{\gamma+\pi/2}(\pi). \tag{A7}$$

Consider now the line through the origin in the xy plane that is the intersection of the xy plane with a plane perpendicular to α and containing the origin. If $\gamma + \pi/2$ is chosen to be the angle which that line makes with the x axis, then

$$R_{\gamma+\pi/2}(-\pi)R(\alpha)R_{\gamma+\pi/2}(\pi) = R(-\alpha). \tag{A8}$$

Equation (A8) implies Eqs. (A3) and (A2). Thus, we have established the generality of Eq. (A1).

In essence, Eq. (A1) demonstrates the equivalence of two coordinate systems for specifying points in $SO(3)$, one in which the coordinates are α_x, α_y, and α_z, the other in which the coordinates are γ, ϵ_x, and ϵ_y. Near the equator, it is possible to derive a linear transformation that relates the two coordinate systems. Suppose a point near the equator is $R(\alpha)$, with

$$\alpha = \alpha_0 + \delta, \tag{A9}$$

$$\alpha_0 = \pi(\cos\gamma, \sin\gamma, 0), \tag{A10}$$

$$\delta_x \sin\gamma - \delta_y \cos\gamma = 0. \tag{A11}$$

δ is the displacement from the equator. Equation (A11) states that δ only as components towards the origin and along z, but not tangent to the equator. To first order in $|\delta|$, $R(\alpha)$ can be written in the form of Eq. (A1) with

$$\epsilon = (-2\delta_z \sin\gamma/\pi + \delta_x \cos^2\gamma + \delta_y \sin\gamma\cos\gamma,$$
$$2\delta_z \cos\gamma/\pi + \delta_x \sin\gamma\cos\gamma + \delta_y \sin^2\gamma, 0). \tag{A12}$$

If $\gamma = 0$, Eq. (A12) indicates that a displacement towards the origin, i.e., a nonzero δ_x, becomes the x component of ϵ. A displacement along z, i.e., a nonzero δ_z, becomes the y component of ϵ. For an arbitrary γ, the component of δ in the direction of the origin becomes the component of ϵ in the direction of the origin. The component of δ along z becomes the component of ϵ in the direction tangent to the equator at α_0.

APPENDIX B: DYNAMICAL CONSEQUENCES OF SYMMETRY IN PHASE SHIFT SCHEMES

1. Motivation

In Sec. IV, we saw that a symmetric phase shift scheme, i.e., an iterative scheme of the form $[\phi_1,\phi_2,\ldots,\phi_2,\phi_1]$, produces a basin image with reflection symmetry in the xy plane of $SO(3)$, as shown in Fig. 13. In Sec. V, the same symmetry was shown to lead to narrowband inversion sequences in which the excitation profile undergoes a progressive, rather than transient, narrowing with successive iterations. These features are attributed to symmetry in the dynamics of the function F on $SO(3)$ that underlies the performance of the iterative schemes. In this Appendix, we give a concise statement and proof of the dynamical symmetry that results from the symmetry of the phase shifts. In addition, we investigate the dynamical properties of schemes in which the phase shifts are antisymmetric, i.e., schemes of the form $[\phi_1,\phi_2,\ldots,-\phi_2,-\phi_1]$. A reflection symmetry with potential value in generating rotations about a constant axis is demonstrated.

2. Symmetric phase shifts

Consider two points $R(\alpha)$ and $R(\alpha')$ in $SO(3)$ related by reflection in the xy plane:

$$\alpha = (\alpha_x,\alpha_y,\alpha_z), \tag{B1}$$

$$\alpha' = (\alpha_x,\alpha_y,-\alpha_z). \tag{B2}$$

Equations (B1) and (B2) are equivalent to the statement

$$R(\alpha)^{-1} = R_z(\pi)R(\alpha')R_z(\pi)^{-1}. \tag{B3}$$

We apply an arbitrary symmetric phase shift scheme to $R(\alpha)$ and $R(\alpha')$, generating the iterate points $R(\beta)$ and $R(\beta')$:

$$R(\beta) = R(\alpha_{\phi_1})R(\alpha_{\phi_2})\cdots R(\alpha_{\phi_2})R(\alpha_{\phi_1}), \tag{B4}$$

$$R(\beta') = R(\alpha'_{\phi_1})R(\alpha'_{\phi_2})\cdots R(\alpha'_{\phi_2})R\alpha'_{\phi_1}), \tag{B5}$$

using the notation of Eq. 14. If $R(\beta)$ and $R(\beta')$ have the same relationship as $R(\alpha)$ and $R(\alpha')$ in Eq. (B3), then they are also related by reflection in the xy plane. In fact,

$$R_z(\pi)R(\beta')R_z(\pi)^{-1}$$
$$= R_z(\pi)R(\alpha'_{\phi_1})R_z(\pi)^{-1}R_z(\pi)R(\alpha'_{\phi_2})R_z(\pi)^{-1}$$
$$\times\cdots R_z(\pi)R(\alpha'_{\phi_2})R_z(\pi)^{-1}R_z(\pi)R(\alpha'_{\phi_1})R_z(\pi)^{-1} \tag{B6}$$
$$= R(-\alpha_{\phi_1})R(-\alpha_{\phi_2})\cdots R(-\alpha_{\phi_2})R(-\alpha_{\phi_1}). \tag{B7}$$

Comparing Eqs. (B7) and (B4), we see that

$$R_z(\pi)R(\beta')R_z(\pi)^{-1} = R(\beta)^{-1}. \tag{B8}$$

The reflection symmetry of the two initial points is preserved in their iterates. Clearly, this holds to all orders of iteration.

An immediate consequence of the reflection symmetry in the dynamics is that initial points in the xy plane of $SO(3)$ must remain in the xy plane upon iteration. A point in the xy plane is certainly related to itself by reflection. Therefore, if such a point were mapped to a point above the xy plane upon iteration, it would necessarily also be mapped to another point symmetrically disposed below the xy plane. But this would contradict the fact that F, the underlying function, is one-to-one.

The above proof also bears on the locus of points in $SO(3)$ that corresponds to a pulse sequence with variations in $\Delta\omega$. For any pulse sequence with symmetric phases, or phase-modulated pulse with an even phase function, it must be the case that the point in $SO(3)$ corresponding to a resonance offset $\overline{\Delta\omega}$ is the reflection in the xy plane of the point corresponding to a resonance offset $-\overline{\Delta\omega}$. This statement is certainly true of a single pulse, as seen from Eq. (12). Any other pulse sequence with symmetric phases can then be considered to be generated from a single pulse by applying a phase shift scheme with symmetric phase shifts. In particular, a pulse sequence with symmetric phases must produce a rotation about an axis in the xy plane on resonance.

C. Antisymmetric phase shifts

If an iterative scheme has antisymmetric phase shifts, the dynamics of F display reflection symmetry in the xz plane. If two points $R(\alpha)$ and $R(\alpha')$ are related by a reflection in the xz plane,

$$\alpha = (\alpha_x,\alpha_y,\alpha_z), \tag{B9}$$

$$\alpha' = (\alpha_x,-\alpha_y,\alpha_z). \tag{B10}$$

Equations (B9) and (B10) are equivalent to

$$R(\alpha)^{-1} = R_y(\pi)R(\alpha')R_y(\pi)^{-1}. \tag{B11}$$

If the first iterate $R(\beta')$ is generated from $R(\beta)$ by an antisymmetric phase shift scheme, then $R(\beta')$ satisfies

$$\begin{aligned} &R_y(\pi)R(\beta')R_y(\pi)^{-1} \\ &= R_y(\pi)R(\alpha_{-\phi_1})R_y(\pi)^{-1}R_y(\pi)R(\alpha'_{-\phi_2})R_y(\pi)^{-1}\cdots \\ &\quad\times R_y(\pi)R(\alpha'_{\phi_2})R_y(\pi)^{-1}R_y(\pi)R(\alpha_{\phi_1})R_y(\pi)^{-1} \qquad \text{(B12)} \\ &= R(\beta)^{-1}, \qquad \text{(B13)} \end{aligned}$$

where $R(\beta)$ is the first iterate of $R(\alpha)$. Thus, $R(\beta')$ and $R(\beta)$ are related by a reflection in the xz plane. The reflection symmetry is preserved to all orders of iteration.

In analogy to the symmetric phase shift case, the reflection symmetry in the xz plane constrains initial points in the xz plane to remain in the xz plane under iteration. Due to the rotational symmetry about the z axis exhibited by all phase shift schemes, initial points in any plane containing the z axis are constrained to that plane under iteration.

If a phase shift scheme is not antisymmetric but can be made antisymmetric by subtracting a constant ϕ_0 from all phase shifts, then the dynamics exhibits reflection symmetry in a plane containing the z axis and with an azimuthal angle ϕ_0.

The locus of points in $SO(3)$ for any pulse sequence with antisymmetric phases, or phase-modulated pulse with an odd phase function, must lie in the xz plane. The locus of points for a single pulse with a phase of zero lies in the xz plane, as may be seen from Eq. (12). Any pulse sequence with antisymmetric phases can be viewed as being generated from a single pulse with a phase of zero by an antisymmetric phase shift scheme.

A potential application of antisymmetric phase shift schemes is in the generation of pulse sequences that produce rotations about a specific axis in the xy plane, i.e., rotations with a constant phase. In general, all invariant sets under a phase shift scheme exhibit rotational symmetry about z, as discussed in Sec. IV B. Thus, it is not possible to make a particular point in the xy plane a stable fixed point without making all other points that are related by a rotation about z also stable fixed points. However, if an antisymmetric phase shift scheme is applied to an initial pulse sequence for which the locus of initial points in $SO(3)$ lies in a plane containing the z axis, e.g., a single pulse, then the relevant dynamics are restricted to that plane. If a point in the xy plane is stable, all initial points in the basin will converge to precisely the same point. Thus, sequences for broadband excitation without signal phase variations may be generated. The significance of such sequences is discussed in Ref. 9. One example of an antisymmetric scheme for broadband population inversion is [256,52,0,128,0, − 128,0, − 52, − 256].

APPENDIX C: THE RELATIONSHIP OF AVERAGE HAMILTONIAN THEORY TO A FIXED POINT ANALYSIS

Iterative schemes for selective multiple quantum excitation and for heteronuclear decoupling in liquids were originally developed using coherent averaging theory. In Sec. VI, we showed that the same schemes could be analyzed with fixed point methods. The question naturally arises: is there a general connection between the two theoretical approaches? Here we demonstrate such a connection. In particular, we show that an iterative scheme with a superstable fixed point generates pulse sequences whose propagators equal the desired propagator to increasingly high order in the sense of average Hamiltonian theory. This connection is implicit for the simple $SO(3)$ case of a single spin-1/2 in comparing the work of Levitt, Freeman, and Frenkiel[3] and Waugh.

Consider an iterative scheme that is equivalent to a function on the propagator space for a given spin system. The scheme generates pulse sequences S_1, S_2, etc. from an initial sequence S_0. The Hamiltonian during the ith sequence is assumed to be of the form

$$\mathcal{H}_i(t,\lambda) = A_i(t) + \lambda B_i(t), \tag{C1}$$

where $A_i(t)$ represents the dominant interaction, $B_i(t)$ represents a perturbation, and λ is an experimental parameter. The precise nature of the Hamiltonian terms is unimportant, but as a typical example $A_i(t)$ might be the rf field interaction, $B_i(t)$ a spin coupling, and λ the coupling constant. In other examples, $\lambda B_i(t)$ could be a resonance offset or rf inhomogeneity term. The sequence S_i has a propagator $U_i(t,\lambda)$. With τ_i being the total length of S_i, it is further assumed that $U_i(\tau_i, 0) = U_0(\tau_0, 0)$, i.e., that the propagator for the initial sequence when $\lambda = 0$ is a fixed point of the scheme.

An average Hamiltonian theory analysis of the pulse sequences would proceed by writing the propagators in the form

$$U_i(t,\lambda) = U_i(t,0)V_i(t,\lambda). \tag{C2}$$

$V_i(t,\lambda)$ is the propagator in the interaction representation defined by $A_i(t)$, i.e., the propagator for the Hamiltonian

$$\lambda\tilde{B}_i(t) = \lambda U_i(t,0)^{-1}B_i(t)U_i(t,0). \tag{C3}$$

$V_i(\tau_i,\lambda)$ can be expanded using the Magnus formula:

$$\begin{aligned} V_i(\tau_i,\lambda) = \exp[&-i(\lambda B_i^{(0)} + \lambda^2 B_i^{(1)} \\ &+ \lambda^3 B_i^{(2)} + \cdots)\tau_i]. \end{aligned} \tag{C4}$$

It might then be shown, possibly using theorems developed by Burum *et al.*[30] and Warren *et al.*,[2] that the Magnus expansion terms $B_i^{(j)}$ vanish for $0 \leqslant j \leqslant k_i$, with k_i increasing as i increases. Thus, $V_i(\tau_i,\lambda)$ is approximately the unit operator for a range of values of λ that grows with successive iterations. $U_i(\tau_I,\lambda)$ then approximates the desired propagator $U_0(\tau_0, 0)$ for an increasing range of values of λ upon iteration.

Our goal is now to show that the above scenario is guaranteed to apply if $U_0(\tau_0, 0)$ is a superstable fixed point of the iterative scheme. In other words, we seek to prove that iteration ensures the disappearance of Magnus expansion terms up to an order k_i that increases with i, without referring to the details of the spin system, the iterative scheme, or the pulse sequence. To do so, we make use of the following theorem: the terms $B_i(j)$ vanish for $0 \leqslant j \leqslant k_i$ if and only if the derivatives

$$\left.\frac{d^n U_i(\tau_i,\lambda)}{d\lambda^n}\right|_{\lambda=0}$$

vanish for $1 \leqslant n \leqslant k_i + 1$. The theorem applies to any sequence S_i with a Hamiltonian as in Eq. (C1), not only to sequences generated iteratively. The theorem is proved most

directly by combining Eqs. (C2) and (C4) and expanding the exponential in Eq. (C4) in a Taylor series. The utility of the theorem in the current context is that it reduces the problem to an investigation of the derivatives of $U_i(\tau_i, \lambda)$.

To treat the derivatives of $U_i(\tau_i, \lambda)$, we choose the form

$$U_i(\tau_i, \lambda) = \exp[-i\mathbf{C}_i(\lambda)\cdot\mathbf{Q}]. \tag{C5}$$

The components of $\mathbf{Q}$, namely $\{Q_m\}$, are Hermitian operators such that Eq. (C5) is a general expression for unitary operators in the propagator space. The components of $\mathbf{C}_i(\lambda)$, which are real, are coordinates of $U_i(\tau_i, \lambda)$ in the propagator space. For a spin system, there is a finite number n of components. The function that underlies the iterative scheme can be considered to be a function F that acts on the n-vectors $\mathbf{C}_i(\lambda)$:

$$\mathbf{C}_i(\lambda) = F^i[\mathbf{C}_0(\lambda)]. \tag{C6}$$

Since $U_0(\tau_0, 0)$ is a fixed point, we define $\bar{\mathbf{C}}$ to be $\mathbf{C}_0(0)$ and have

$$\mathbf{C}_i(0) = \bar{\mathbf{C}}. \tag{C7}$$

We assume that F may be expanded in a Taylor series about $\bar{\mathbf{C}}$:

$$F(\mathbf{C}) = F(\bar{\mathbf{C}}) + D(F)(\mathbf{C}-\bar{\mathbf{C}}) + \tfrac{1}{2}D^2(F)(\mathbf{C}-\bar{\mathbf{C}})(\mathbf{C}-\bar{\mathbf{C}}) + \cdots. \tag{C8}$$

In Eq. (C8), the arguments λ and the subscripts i have been dropped for simplicity. The notation $D^m(F)$ represents the mth derivative of F with respect to $\mathbf{C}$ evaluated at $\bar{\mathbf{C}}$, which is a matrix with n^{m+1} elements. Multiplication of an n-vector by an n^l-element matrix is defined so that the product is an n^{l-1}-element matrix.

The assumption that $U_0(\tau_0, 0)$ is a superstable fixed point implies that the eigenvalues of $D(F)$, the Jacobian of F at $\bar{\mathbf{C}}$, are zero. For the moment, we adopt the stricter requirement that $D(F)$ vanish entirely. With this requirement

$$F(\mathbf{C}) = \bar{\mathbf{C}} + \tfrac{1}{2}D^2(F)(\mathbf{C}-\bar{\mathbf{C}})(\mathbf{C}-\bar{\mathbf{C}}) + \cdots. \tag{C9}$$

The leading term in the difference $F(C)-\bar{\mathbf{C}}$ involves the second power of $(\mathbf{C}-\bar{\mathbf{C}})$. Using Eq. (C9) and substituting $F(\mathbf{C})$ for $\mathbf{C}$, we find

$$F^2(\mathbf{C}) = \bar{\mathbf{C}} + \tfrac{1}{8}D^2(F)[D^2(F)(\mathbf{C}-\bar{\mathbf{C}})(\mathbf{C}-\bar{\mathbf{C}})] \times [D^2(F)(\mathbf{C}-\bar{\mathbf{C}})(\mathbf{C}-\bar{\mathbf{C}})] + \cdots. \tag{C10}$$

The leading term in the difference $F^2(\mathbf{C}) - \bar{\mathbf{C}}$ involves the fourth power of $(\mathbf{C}-\bar{\mathbf{C}})$. Thus $D(F^2)$, $D^2(F^2)$, and $D^3(F^2)$, the derivatives of the function F^2 with respect to $\mathbf{C}$ evaluated at $\bar{\mathbf{C}}$, must all vanish. Continuing in this way, it can be shown that the derivatives $D^m(F^i)$ vanish for $1 \leqslant m \leqslant 2^i - 1$.

Next, we turn to the derivatives of $\mathbf{C}_i(\lambda)$ with respect to λ. Using the chain rule and Eq. (C6),

$$\left.\frac{d\mathbf{C}_i(\lambda)}{d\lambda}\right|_{\lambda=0} = D(F^i)\left.\frac{d\mathbf{C}_0(\lambda)}{d\lambda}\right|_{\lambda=0}, \tag{C11}$$

$$\left.\frac{d^2\mathbf{C}_i(\lambda)}{d\lambda^2}\right|_{\lambda=0} = D^2(F^i)\left(\frac{d\mathbf{C}_0(\lambda)}{d\lambda}\right)\left(\frac{d\mathbf{C}_0(\lambda)}{d\lambda}\right)\Bigg|_{\lambda=0} + D(F^i)\left.\frac{d^2\mathbf{C}_0(\lambda)}{d\lambda^2}\right|_{\lambda=0}. \tag{C12}$$

Similarly, the m^{th} derivative of $\mathbf{C}_i(\lambda)$ can be written as a sum of terms that are products of derivatives of F^i with respect to C and derivatives of $\mathbf{C}_0(\lambda)$ with respect to λ. The highest derivative of F^i that appears is $D^m(F^i)$. Therefore, we arrive at the important result that the nth derivative of $\mathbf{C}_i(\lambda)$ vanishes at $\lambda = 0$ for $1 \leqslant m \leqslant 2^i - 1$.

We are now in a position to examine the derivatives of $U_i(\tau_i, \lambda)$. It can be shown by expanding the exponential in Eq. (C5) that the vanishing of the derivatives of $\mathbf{C}_i(\lambda)$ implies that

$$\left.\frac{d^m U_i(\tau_i, \lambda)}{d\lambda^m}\right|_{\lambda=0} = 0, \quad 1 \leqslant m \leqslant 2^j - 1. \tag{C13}$$

Then, using the theorem stated above, the Magnus expansion terms $B_i^{(j)}$ vanish for $0 \leqslant j \leqslant 2^i - 2$. This is the desired result, that the iterative scheme generates pulse sequences with propagators that are independent of the perturbation $\lambda B_i(t)$ in Eq. (C1) to increasingly high order in the sense of coherent averaging theory.

If $D(F)$ in Eq. (C8) is not zero, but has all its eigenvalues equal to zero, then there is an integer k such that $D(F^k)$ vanishes. Then Eq. (C13) holds with i replaced by i/k when i is a multiple of k. The order to which the Magnus expansion terms vanish increases with every k iterations.

[1] R. Tycko and A. Pines, Chem. Phys. lett. **111**, 462 (1984).
[2] W. S. Warren, D. P. Weitekamp, and A. Pines, J. Chem. Phys. **73**, 2084 (1980).
[3] M. H. Levitt, R. Freeman, and T. Frenkiel, in *Advances in Magnetic Resonance*, edited by J. S. Waugh (Academic, New York, 1983) Vol. 11.
[4] J. S. Waugh, J. Magn. Reson. **49**, 517 (1982).
[5] M. H. Levitt and R. R. Ernst, J. Magn. Reson. **55**, 247 (1983).
[6] A. J. Shaka and R. Freeman, J. Magn. Reson. **59**, 169 (1984).
[7] (a) The term propagator refers to the quantum mechanical propagator when discussing quantum states, $|t\rangle$, i.e., evolution in Hilbert space and to the superpropagator or Liouvillian when discussing quantum statistical states $\rho(t)$, i.e., evolution in Liouville space. (b) R. Tycko, Phys. Rev. Lett. **51**, 775 (1983).
[8] R. Tycko, E. Schneider, and A. Pines, J. Chem. Phys. **81**, 680 (1984).
[9] R. Tycko, H. M. Cho, E. Schneider, and A. Pines, J. Magn. Reson. **61**, 90 (1985).
[10] J. Baum, R. Tycko, and A. Pines, J. Chem. Phys. **79**, 4643 (1983).
[11] J. Baum, R. Tycko, and A. Pines (in preparation).
[12] T. M. Barbara, R. Tycko, and D. P. Weitekamp, J. Magn. Reson. **62**, 54 (1985).
[13] M. H. Levitt and R. Freeman, J. Magn. Reson. **33**, 473 (1979).
[14] R. Freeman, S. P. Kempsell, and M. H. Levitt, J. Magn. Reson. **38**, 453 (1980).
[15] M. H. Levitt and R. Freeman, J. Magn. Reson. **43**, 65 (1981).
[16] M. H. Levitt, J. Magn. Reson. **48**, 234 (1982).
[17] M. H. Levitt, J. Magn. Reson. **50**, 95 (1982).
[18] A. J. Shaka and R. Freeman, J. Magn. Reson. **55**, 487 (1983).
[19] M. H. Levitt, D. Suter, and R. R. Ernst, J. Chem. Phys. **80**, 3064 (1984).
[20] J. Baum, R. Tycko, and A. Pines (in preparation).
[21] R. Tycko and A. Pines, J. Magn. Reson. **60**, 156 (1984).
[22] A. J. Shaka, J. Keeler, M. B. Smith, and R. Freeman, J. Magn. Reson. **61**, 175 (1985).
[23] U. Haeberlen, *High Resolution NMR in Solids: Selective Averaging* (Academic, New York, 1976).
[24] M. Mehring, *Principles of High Resolution NMR in Solids*, 2nd ed. (Springer, New York, 1983).
[25] J. S. Waugh, L. M. Huber, and U. Haeberlen, Phys. Rev. Lett. **20**, 180 (1968).
[26] U. Haeberlen and J. S. Waugh, Phys. Rev. **175**, 453 (1968).
[27] P. Mansfield, J. Phys. C **4**, 1444 (1971).
[28] W.-K. Rhim, D. D. Elleman, and R. W. Vaughan, J. Chem. Phys. **59**, 3740 (1973).
[29] W.-K. Rhim, D. D. Elleman, L. B. Schreiber, and R. W. Vaughan, J. Chem. Phys. **60**, 4595 (1974).

[30]D. P. Burum and W.-K. Rhim, J. Chem. Phys. **71**, 944 (1979).
[31]D. P. Burum, M. Linder, and R. R. Ernst, J. Magn. Reson. **44**, 173 (1981).
[32]F. Bloch, Phys. Rev. **93**, 944 (1954).
[33]M. H. Levitt and R. Freeman, J. Magn. Reson. **43**, 502 (1981).
[34]M. H. Levitt, R. Freeman, and T. Frenkiel, J. Magn. Reson. **47**, 328 (1982).
[35]M. H. Levitt, R. Freeman, and T. Frenkiel, J. Magn. Reson. **50**, 157 (1982).
[36]J. S. Waugh, J. Magn. Reson. **50**, 30 (1982).
[37]A. J. Shaka, J. Keeler, T. Frenkiel, and R. Freeman, J. Magn. Reson. **52**, 335 (1983).
[38]A. J. Shaka, J. Keeler, and R. Freeman, J. Magn. Reson. **53**, 313 (1983).
[39]G. Bodenhausen, Prog. Nucl. Magn. Reson. Spectrosc. **14**, 137 (1981).
[40]D. P. Weitekamp, in *Advances in Magnetic Resonance*, edited by J. S. Waugh (Academic, New York, 1983), Vol. 11.
[41]H. Hatanaka, T. Terao, and T. Hashi, J. Phys. Soc. Jpn. **39**, 835 (1975).
[42]G. Drobny, A. Pines, S. Sinton, D. P. Weitekamp, and D. Wemmer, Symp. Faraday Soc. **13**, 49 (1979).
[43]A. Pines, M. G. Gibby, and J. S. Waugh, J. Chem. Phys. **59**, 569 (1973).
[44]S. R. Hartman and E. L. Hahn, Phys. Rev. **128**, 2042 (1962).
[45]G. A. Morris and R. Freeman, J. Am. Chem. Soc. **101**, 760 (1979).
[46]D. T. Pegg, D. M. Doddrell, and M. R. Bendall, J. Chem. Phys. **77**, 2745 (1982).
[47]W.-K. Rhim, A. Pines, and J. S. Waugh, Phys. Rev. B **3**, 684 (1971).
[48]F. Bloch, Phys. Rev. **70**, 460 (1946).
[49]S. Vega and A. Pines, J. Chem. Phys. **66**, 5624 (1977).
[50]A. Wokaun and R. R. Ernst, J. Chem. Phys. **67**, 1752 (1977).
[51]S. Vega, J. Chem. Phys. **68**, 5518 (1978).
[52]J. R. Garbow, Ph.D. dissertation, University of California, Berkeley, 1983, Lawrence Berkeley Laboratory Report No. 16119.
[53]O. W. Sørensen, G. W. Eich, M. H. Levitt, G. Bodenhausen, and R. R. Ernst, Prog. Nucl. Magn. Reson. Spectrosc. **16**, 163 (1983).
[54](a) I. Percival and D. Richards, *Introduction to Dynamics* (Cambridge University, Cambridge, 1982); (b) P. Collet and J. P. Eckman, *Iterated Maps on the Interval as Dynamical Systems* (Birkhauser, Boston, 1980).
[55]J. Guckenheimer and P. Holmes, *Nonlinear Oscillations, Dynamical Systems, and Birfurcations of Vector Fields* (Springer, New York, 1983).
[56]"Nonlinear Dynamics", Ann. N.Y. Acad. Sci. **357**, (1980), edited by R. H. G. Helleman
[57]A. Abragam and M. Goldman, *Nuclear Magnetism: Order and Disorder* (Oxford University, New York, 1982).
[58]M. J. Feigenbaum, in Los Alamos Science, Summer 1980, p. 4.
[59]R. M. May, Nature **261**, 459 (1976).
[60]R. P. Feynman, F. L. Vernon, and R. W. Hellwarth, J. Appl. Phys. **28**, 49 (1957).
[61]L. Allen and J. H. Eberly, *Optical Resonance and Two-Level Atoms* (Wiley, New York, 1975).
[62]M. I. Petrashen and E. D. Trifonov, *Applications of Group Theory in Quantum Mechanics* (M.I.T., Cambridge, 1969).
[63]M. Hammermesh, *Group Theory and Its Application to Physical Problems* (Addison–Wesley, Menlo Park, 1962).
[64]B. Mandelbrot, *Fractals: Form, Chance, and Dimension* (Freeman, San Francisco, 1977).
[65]M. H. Levitt and R. R. Ernst, Mol. Phys. **50**, 1109 (1983).
[66]B. L. Silver, *Irreducible Tensor Methods* (Academic, New York, 1976).
[67]H. M. Cho, R. Tycko, and A. Pines (in preparation).
[68]W. Magnus, Commun. Pure Appl. Math. **7**, 649 (1954).
[69]P. Pechukas and J. C. Light, J. Chem. Phys. **44**, 3897 (1966).
[70]R. M. Wilcox, J. Math. Phys. **8**, 962 (1967).
[71]I. Bialynicki-Birula, B. Mielnik, and J. Plebanski, Ann. Phys. **51**, 187 (1969).
[72]R. Tycko, Ph.D. dissertation, University of California, Berkeley, 1984, Lawrence Berkeley Laboratory Report No. 18475.